https://doi.org/10.1016/j.enconman.2021.113899

Methanol to power through high-efficiency hybrid fuel cell system: Thermodynamic, thermo-economic, and techno-economic (3T) analyses in Northwest China

Zhen Wu[a,b], Pengfei Zhu[a], Leilei Guo[a], Jing Yao[a], Jianwei Ren[c], Sandra Kurko[d], Zaoxiao Zhang[a,e,*], Meng Ni[b,f,*]

[a]Shaanxi Key Laboratory of Energy Chemical Process Intensification, School of Chemical Engineering and Technology, Xi'an Jiaotong University, Xi'an, China

[b]Building Energy Research Group, Department of Building and Real Estate, The Hong Kong Polytechnic University, Hung Hom, Kowloon, Hong Kong, China

[c]Department of Mechanical Engineering Science, Faculty of Engineering and the Built Environment (FEBE)，University of Johannesburg, Johannesburg, South Africa

[d]Center of Excellence for Hydrogen and Renewable Energy, Vinča Institute of Nuclear Sciences, University of Belgrade, Belgrade, 11351, Serbia

[e]State Key Laboratory of Multiphase Flow in Power Engineering, Xi'an Jiaotong University, Xi'an, China

[f]Environmental Energy Research Group, Research Institute for Sustainable Urban Development (RISUD), The Hong Kong Polytechnic University, Hung Hom, Kowloon, Hong Kong, China

*Corresponding author, Email: zhangzx@mail.xjtu.edu.cn (Z Zhang) meng.ni@polyu.edu.hk (M Ni)

ABSTRACT: Advanced efficient energy conversion technology using clean alternative fuel contributes to the alleviation of the energy crisis and environmental deterioration. In this situation, a novel methanol utilization technology for power generation based on hybrid fuel cell system,

consisting of a solid oxide fuel cell (SOFC), a gas processing unit (GP) and a proton exchange membrane fuel cell (PEMFC) is proposed in this work. Thermodynamic analysis of the system shows that the energy conversion efficiency and exergy efficiency are both higher than the previously reported standalone or hybrid energy systems using methanol as fuel, which are 68.6% and 60.8% respectively. Besides, no recirculation ratio of anode off-gas and moderate fuel utilization of about 0.5 are suggested for the SOFC component to balance the power distribution and improve the efficiency. Afterwards, this hybrid fuel cell system is also investigated from thermo-economic and techno-economic perspectives. Take Northwest China as a case, the 1 MWe methanol-fed power plant has a specific electric energy cost of 0.5594 CNY/kWh, much lower than the methanol steam reforming-PEMFC power plant (2.4 CNY/kWh). At the same time, the sensitivity analyses reveal that the cost of the hybrid power system is not sensitive to the market price fluctuation. With financial subsidies for existing renewable power plants, the payback period can be shortened to 1.4 year and the annual return on investment is about 3.58%. These results reveal that this two-stage fuel cell hybrid system is a kind of efficient and economical methanol to power conversion technology, especially for small power scale.

Keywords: Fuel cell; Hybrid power system; Methanol fuel; High efficiency; Performance evaluation

Nomenclature

Abbreviation

CFPP	coal fired power plant
CNY	China Yuan
DMFC	direct methanol fuel cell

DIR	direct internal reforming
FC	fuel cell
GP	gas processing
HC	hydrocarbon
HEX	heat exchanger
HT-WGS	high temperature-water gas shift
LHV	low heat value
LT-WGS	low temperature-water gas shift
MCFC	molten carbonate fuel cell
mCCHP	combined cooling heating and power
MD	methanol decomposition
mGT	micro gas turbine
MH	metal hydride
MSR	methanol steam reforming
MTST	mid-temperature solar thermochemical
PEMFC	proton exchange membrane fuel cell
S/C	steam-to-methanol ratio
SEEC	specific electric energy cost
SI	spark ignition
SOFC	solid oxide fuel cell
TSA	thermal swing adsorption

YSZ yttria stabilization zirconia

Symbols

A	area, m^2
C	cost, USD/CNY
Cp	specific heat capacity, J kg^{-1} K^{-1}
C_d	reaction rate constant for hydrogen desorption, s^{-1}
D^{eff}	effective diffusion coefficient, m s^{-1}
E_{act}	activation energy, J mol^{-1}
E_N	reversible voltage, V
F	Faraday constant, C mol^{-1}
f	factor, %
$\frac{H}{M}$	atomic ratio of hydrogen to metal
I	current, A
J	current density, A m^{-2}
J_0	exchange current density, A m^{-2}
K	reaction equilibrium constant
k	frequency factor of catalyst, kmol kg^{-1} s^{-1} bar^{-1}
L_{Pt}	amount of catalyst Pt load, mg cm^{-2}
l	thickness, mm
$\dot{m}_{H_2}$	H_2 flow velocity, mol s^{-1}
n_{cycle}	number of cycles
P	power, kW
p	pressure, bar
r	reaction rate, mol s^{-1}
R_g	universal gas constant, J K^{-1} mol^{-1}
T	temperature, K

t	time, h
V	voltage, V
W	volume, m^3
X	reaction fraction

Greek

δ_{O_2}	oxygen percent in the fuel
ϕ	mass or molar flow, kg/s or mol/s
η	energy efficiency
γ	compression ratio
ρ	density, kg/m3
χ	price of methanol fuel
μ	fuel utilization
$\triangle H$	reaction enthalpy, kJ mol^{-1}
λ	cycle life, year
ω_{MH}	hydrogen capacity, wt%
ε	porosity
θ	tortuosity
α	partial pressure order

Subscript

a	anode
act	activation
AUX	auxiliary
c	cathode
Capi	capital
Cata	catalyst
comp	compressor
conc	concentration

cool	coolant
Depr	depreciation
e	electrolyte
emp	empty
eq	equilibrium
Gross	gross
h	high-temperature
hot	hot fluid
in	inlet
ISC	isentropic
Ins	insurance
Int	interest
INV	inverter
l	low-temperature
max	maximum
Main	maintenance
MEC	mechanical
Net	net
ohm	ohmic
oper	operation
PEM	proton exchange membrane
reac	reactor
ref	reference
sat	saturated
WGS-cata	catalyst of water gas shift reaction
WGS-reac	water gas shift reactor

1. Introduction

The overuse of traditional fossil fuels causes severe global issues, such as energy crisis, greenhouse gas emission and environmental pollution [1,2]. However, the fast pace of human development requires a large demand in energy, especially the electricity power which is mostly generated from the coal fired power plant in China. Therefore, clean alternative fuels for power generation are urgently needed, which can contribute to the sustainable development of human society and ecological environment [3,4]. Methanol is viewed as an important alternative fuel even the optimal secondary energy in the opinion of the Nobel Laureates Dr. George A. Olah [5], because it is a green and clean energy with high energy density. It is well known that methanol can be derived from plant cellulose via distillation and coal-to-methanol, strongly indicating the abundant source. In 2016, the global production capacity of methanol reached 129 million metric tons per year, among which China contributed more than 60%. Moreover, the production technology of methanol is very mature and the generation cost is lower than those of gasoline and diesel fuels. For the liquid methanol (room temperature) used for practical applications, it is also easy to store and transport to the terminal by pipeline and liquid tank. In such context, the methanol as a fuel has been attracting more and more attention for power generation. Especially in China, the production capacity of methanol is estimated to be 100 million metric tons in 2020 due to the encouraged development of methanol vehicles [6]. Therefore, it is of great significance and value to promote the development of methanol energy and methanol economy to realize high efficiency power generation using methanol on a large scale.

In the 1920s, Germany first used the methanol as a fuel. The earliest application of methanol as a fuel is the substitute fuel of gasoline for vehicles. Actually, Chinese government initiated a pilot

project employing the methanol vehicles in the regions of Shanghai city, Shaanxi, Shanxi, Guizhou, and Gansu provinces in 2014 and all the pilot methanol vehicles were examined in the result of reaching the acceptance level in 2017. Therefore, a mass of efforts have been attempted on the methanol vehicles technology all over the world. Wu et al. [7] studied the lean-burn limits of engine using gasoline or methanol as a fuel by experiment. It was found that the methanol fueled engine has better lean burn performance than the traditional gasoline engine. The thermal efficiency can reach as high as 24.7%. Moreover, the emissions of hydrocarbon, carbon monoxide and nitrogen oxides are reduced in the methanol engine compared with the gasoline engine. Gong et al. [8] further employed the hydrogen enriched methanol for the lean-burn. When the hydrogen ratios was 3% and 6%, the COV_{imep} (Coefficient of variation in indicated mean effective pressure)) can be decreased by 21.5% and 36.8%, respectively. Additionally, hydrogen addition helps to further decrease HC and CO emissions at low engine speed. Nidhi and Subramanian [9] introduced the oxygen enriched air strategy into the methanol engine. It was found that the highly oxygen enriched air (60.4%) led to very low emissions of HC, CO, and NO_x and the significant increase of thermal efficiency by 20.5%. Although the methanol engine technology for power generation has achieved remarkable progress on improving the efficiency and lowering the emissions, the thermal efficiency of this kind of methanol utilization technology is still low. Recently, the highest thermal efficiency of the engine fueled by methanol with a high compression ratio of 16 and exhaust gas recirculation to improve the efficiency was reported to be as high as 43%~45% [10,11], which is no more than 50%. Therefore, the advanced high-efficiency methanol utilization technology is an urgent need to promote large scale application of the methanol energy.

The fuel cell (FC) can directly convert the chemical energy of the fuel into electric energy by electrochemical reaction without being restricted by the Carnot cycle, so it has the merits of high efficiency, no noise pollution and less emission. From the view of saving energy and protecting environment, fuel cell is the most promising power generation technology [12–15]. The FCs with different electrolytes can be mainly classified as solid oxide fuel cell (SOFC), proton exchange membrane fuel cell (PEMFC), alkaline fuel cell (AFC), phosphoric acid fuel cell (PAFC), and molten carbonate fuel cell (MCFC) [16]. In all types of FCs, PEMFC using pure hydrogen fuel is the most commercial fuel cell due to its moderate operating temperature, superior dynamics, and mature fabrication technology [17]. Herdem et al. [18] employed the methanol reformate gas as the fuel of high-temperature PEMFC. It was found that the maximum efficiency of this system with the power output of 350 W is about 35% at the temperature as high as 180 ℃. Baak et al. [19] further evaluated the techno-economic performance of the combination system of methanol steam reforming and PEMFC (MSR-PEMFC) as energy storage system. The levelized cost of storage was preliminarily estimated to be about 0.34 USD/kWh without considering the variable operational costs, which is much higher than the cost 0.24~0.25 USD/kWh for the transcritical or supercritical CO_2 gas turbine. Besides hydrogen fuel, this kind of fuel cell also can run with methanol, which is called as direct methanol fuel cell (DMFC). However, the energy conversion efficiency as well as power density are not high for the DMFC, because the electrochemical activity of methanol is much lower than the hydrogen electrochemical activity. Jiang et al. [20] employed the ordered electrode (order-structured catalyst layer) instead of agglomerate electrode for the DMFC. The peak power density was found to be increased by 46.6% owing to the lowered polarization losses. Hu et al. [21]

introduced non-uniform cross-sectional serpentine channel into DMFC to facilitate methanol transportation. A significant increase of 18.4% in the power generation was achieved in experiment. However, how to increase the efficiency and avoid the crossover of methanol through proton exchange membrane from the anode to the cathode are still crucial issues to promote the large-scale application of DMFC.

In addition to DMFC, SOFC generally operates at higher temperatures, which makes reforming and shift reactions can be occurred, increasing the fuel flexibility of SOFC [22,23]. Laosiripojana et al. [24] first explored the possible use of methane, methanol, and ethanol fuels in a internal reforming SOFC (DIR-SOFC) over Ni/YSZ catalysts. It was found that the methane and methanol can be used as the direct fuel for the DIR-SOFC at high temperatures while ethanol does not work. Liu et al. [25] further developed direct methanol liquid fueled SOFC and conducted the long-term test. The maximum power density was found to be 698 mW/cm^2 at 650 ℃, which is higher than the value (467 mW/cm^2) of ammonia fuel but lower than that (870 mW/cm^2) of hydrogen fuel. Besides, the methanol-fueled SOFC without notable degradation presented high stable performance, because of no anode coking during long cycles. Strazza et al. [26] evaluated the environmental impact of methanol-fueled SOFC as an auxiliary power system of commercial vessels based on life cycle assessment. The result revealed that this kind of SOFC had extremely lower environmental impact compared with the conventional auxiliary power system (i.e. diesel engine). However, the electrical efficiency of methanol-fed SOFC is not high, which was reported to be about 50% in a maximum [27,28]. In fact, SOFC off-gas still has a certain amount of thermal and underutilized chemical energy which is directly discharged. This is also why the energy conversion efficiency of standalone

SOFC is relatively low. In order to enhance the SOFC performance, the unconsumed fuels with waste heat can be recycled by combining with other energy systems to form hybrid power system. Recently, more and more attention has been focusing on the hybrid power system. Chen et al. [29] developed a novel hybrid power system (MSR-PEMFC-mCCHP) consisting of the geothermal-assisted methanol reforming, PEMFC and micro-CCHP. Through the thermodynamic and economic assessment, a high energy efficiency of 66.3% was achieved with the levelized cost of energy of 0.0422 USD/kWh. Cocco and Tola [30] integrated externally reformed SOFC and micro gas turbine (mGT) for small power scale of 200~500 kW. The methanol-fed SOFC-mGT has a maximum energy efficiency of about 67.8% at the SOFC temperature of 900 ℃, which is slightly higher than the above-mentioned MSR-PEMFC-mCCHP hybrid system. The improvement of hybrid power system efficiency is mainly due to the recovery of waste heat. In addition to power generation, SOFC also plays a role of fuel reformer, which can generate hydrogen via reforming reaction. The produced H_2 delivered into the PEMFC could further improve the efficiency due to additional power generation after the sequential H_2 production and purification processes. Compared to the SOFC-mGT system, the SOFC-PEMFC hybrid system may be more efficient and cleaner for power generation, because the FC usually has higher efficiency and lower emissions due to electrochemical reaction than the GT. Therefore, it is of great significance to explore a new mode of efficient, clean and low-cost utilization of methanol based on hybrid fuel cell power generation technology [31].

In this research work, a novel FC hybrid system fueled by methanol consisting of SOFC, GP unit for H_2 production and purification, and PEMFC, was proposed. Then, thermodynamic, thermo-economic, and techno-economic (3T) modeling of the hybrid power system was applied to

assess the energy conversion performance and economic feasibility of this novel system for practical application as power plant. In addition, the economic analysis is based on the relevant policies and methanol price in Northwest China. The research results are conducive to the promotion and development of novel hybrid fuel cell system for efficient conversion and utilization of methanol.

2. System description

The proposed coupling high and low temperature fuel cell hybrid system using methanol as fuel is designed and illustrated in Fig. 1, which is composed of three subsystems: SOFC, GP, and PEMFC. The SOFC and PEMFC subsystems are mainly responsible for electricity production. The role of GP is aiming at H_2 production and purification by WGS and TSA units, thus serves as a bridge between SOFC and PEMFC. Herein, we name the proposed hybrid power system as SOFC-GP-PEMFC. The working principle can be summarized briefly as follows.

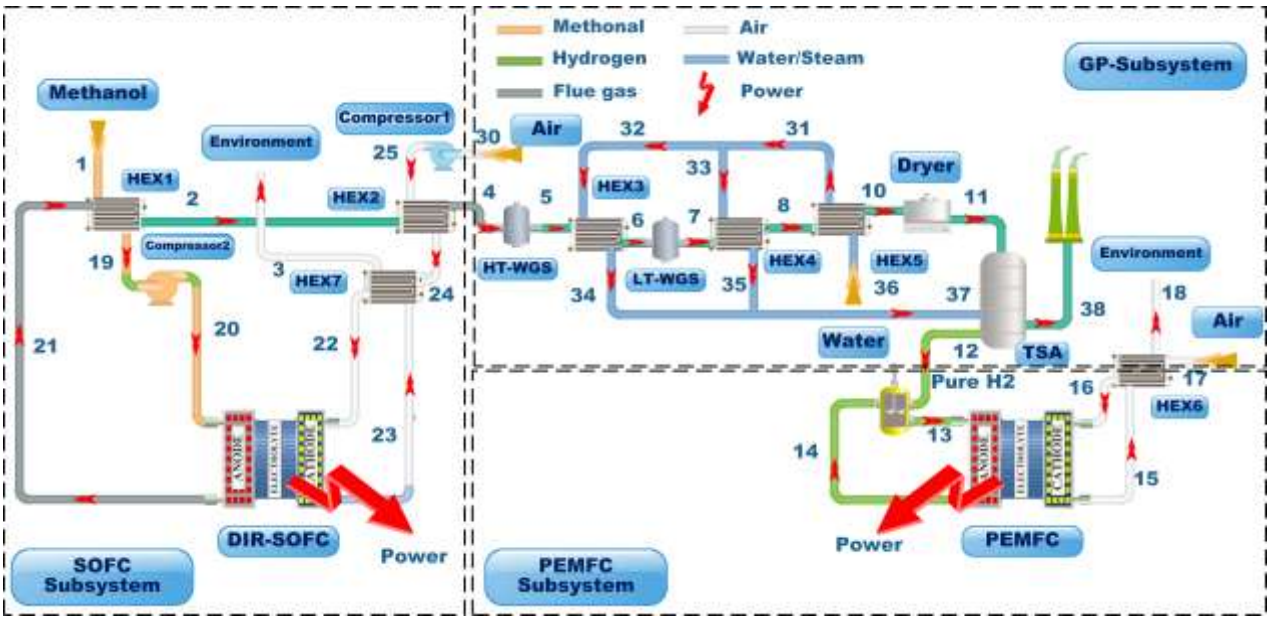

Fig. 1. Operation flowsheet of the SOFC-GP-PEMFC hybrid energy conversion system using methanol as fuel for power generation.

Liquid methanol is preheated and converted into methanol gas by HEX1 with the heat provided by SOFC anode exhaust (path line 21). Similarly, the air is first pumped by blower and then preheated in sequence by the waste heat from the SOFC anode and cathode through HEX2 and HEX7 (path line 2 and 23). Inside the SOFC component, the preheated methanol first goes through the direct internal reforming reaction and then reacts with O_2 from the preheated air in electrochemical reaction for power generation. Concomitantly, the heat carried by SOFC off-gas is recovered to preheat the imported methanol and air. Besides the waste heat exhausting from the SOFC, a part of unconsumed syngas fuel (CO and H_2) is included in the anode off-gas. For the sake of increasing the concentration of hydrogen in the imported fuel of PEMFC, a high-low temperature two-stage WGS unit is employed. Herein, the high temperature WGS contributes to fast H_2 conversion rate while the low temperature WGS ascertains large H_2 conversion ratio due to the exothermic reaction for WGS. It is exactly because of exothermic reaction that the WGS waste heat could be recycled for the follow-up TSA process for H_2 purification as heat source by HEX3, HEX4, and HEX5 through path line 34, 35, and 37. Accordingly, pure H_2 with certain temperature is released from the MH bed of TSA reactor, which enters the PEMFC as anode fuel through path line 12 and 13. It should be noted that the hydrogen remaining in the exhaust gas discharged from PEMFC is recycled to improve the electrochemical conversion efficiency of fuel. For PEMFC cathode inlet oxidant, the air is also preheated by the waste heat supplied by cathode off gas for two reasons. On the one hand, the temperature of tail gas exhausting to the environment through path line 18 can be lowered. On the other hand, the waste heat recovery is conducive to increase the thermal

efficiency of the hybrid system. The electrochemical reaction between hydrogen and oxygen occurs within the PEMFC for additional power generation.

3. System modeling

Some basic assumptions are employed to simplify the modeling of the hybrid power system, which are listed follows.

1) All the gases in this work behave as ideal gases.
2) The reactors are well insulated, indicating heat loss is not taken in to account.
3) Pressure drop of fluid flowing in the pipeline is neglected.
4) No carbon deposition is considered within the SOFC [32].
5) In the thermal-economic model, the material deterioration of SOFC due to high temperature is negligible.
6) The SOFC electrochemical and methanol reforming reactions occur in chemical equilibrium state [33]. Besides, the WGS reaction rate can be obtained at a constant temperature [34].
7) For the thermodynamic modeling of SOFC, the direct internal reforming reaction and electrochemical reaction are modeled separately.
8) Carbon monoxide contained in reformed gas inside the SOFC is assumed to preferentially converted into H_2 by WGS reaction rather than electrochemical reaction with O_2 due to the presence of water.
9) In an ideal situation, the relative humidity of the PEMFC is 100% [35].
10) The cost of auxiliary equipment of the SOFC including combustor, mixer and by-pass valves accounts for 10% of the SOFC stack cost [36,37].

3.1. Thermodynamic modeling

3.1.1. SOFC subsystem modeling

Due to the high operating temperature, SOFC can be used as a reformer to convert methanol to CO, CO2 and H_2 in the presence of steam. In the direct internal reforming process, the three high level reactions are considered, including methanol steam reforming (MSR), methanol decomposition reaction (MD), and the WGS reaction. Generally, the three reactions are the rate determining steps of methanol steam reforming process. The corresponding reaction formulas can be written as the following Eqs. (1-3), respectively [38,39]. The optimum steam-to-methanol (S/C) ratio of the MSR was reported to be in the range of 1.3~2.0 [40,41]. Herein, the fixed S/C ratio of 1.4 is employed for the MSR in this work.

MSR: $CH_3OH+H_2O \rightarrow CO_2+3H_2 \quad \Delta H = 49.37\ \mathrm{kJ/mol}$ (1)

MD: $CH_3OH \rightarrow CO+2H_2 \quad \Delta H = 90.47\ \mathrm{kJ/mol}$ (2)

WGS: $CO+H_2O \rightarrow CO_2+H_2 \quad \Delta H = -41.10\ \mathrm{kJ/mol}$ (3)

The gas composition of the product of the methanol reforming process mainly depends on the equilibrium constant of chemical reaction *K*, which is determined by reaction temperature *T*. According to the basic thermochemical data [42], the functional relationship between *K* and *T* can be described by the following equations for the MSR, MD, and WGS reactions.

$$K_{\mathrm{MSR}} = \frac{p_{CO_2} \cdot p_{H_2}^3}{p_{CH_3OH} \cdot p_{H_2O}} = f(T) = \exp(-3.5042\times10^{-11}\cdot T^4 + 1.2775\times10^{-7}\cdot T^3 - 1.8492\times10^{-4}\cdot T^2 + 0.1347\cdot T - 24.7364) \quad (4)$$

$$K_{\mathrm{MD}} = \frac{p_{CO} \cdot p_{H_2}^2}{p_{CH_3OH}} = f(T) = \exp(-9.7199\times10^{-11}\cdot T^4 + 3.2762\times10^{-7}\cdot T^3 - 4.3445\times10^{-4}\cdot T^2 + 0.2847\cdot T - 63.2854) \quad (5)$$

$$K_{\mathrm{WGS}}=\frac{p_{CO_2}\cdot p_{H_2}}{p_{CO}\cdot p_{H_2O}}=f(T)$$
$$=\exp(5.47301\times10^{-12}\cdot T^4-2.57479\times10^{-8}\cdot T^3+4.63742\times10^{-5}\cdot T^2-0.03915\cdot T+13.2097) \quad (6)$$

The electrochemical model of SOFC, which describes the relationship (the polarization curve) between cell voltage and current density, can be expressed as below.

$$V_{\mathrm{SOFC}}=E_{\mathrm{N}}-V_{\mathrm{act}}-V_{\mathrm{ohm}}-V_{\mathrm{conc}} \quad (7)$$

where E_{N} is the reversible voltages of the SOFC, which can be calculated as follows [22].

$$E_{N,SOFC}=1.253-2.4516\times10^{-4}\cdot T-\frac{R_{\mathrm{g}}\cdot T}{4F}\cdot\ln\left(\frac{p_{\mathrm{H_2O}}^2}{p_{\mathrm{H_2}}^2\cdot p_{\mathrm{O_2}}}\right) \quad (8)$$

where R_{g} is the gas constant; F is the Faraday constant; $p_{\mathrm{H_2}}$, $p_{\mathrm{O_2}}$, and $p_{\mathrm{H_2O}}$ stand for the partial pressure of H_2, O_2, and water vapor, respectively.

During the operation of the fuel cell, different types of overvoltage losses will be occurred, including activation overvoltage V_{act}, concentration overvoltage V_{conc} and ohmic overvoltage V_{ohm}. The activation overvoltage is mainly caused by the necessary activation of charge transfer for electrodes, which can be calculated by the Butler-Volmer equation. The SOFC activation overvoltage for the SOFC can be written as follows. Herein, $V_{\mathrm{act,a}}$ and $V_{\mathrm{act,c}}$ represent the activation overvoltage of anode and cathode, respectively [43].

$$V_{\mathrm{act}}=V_{\mathrm{act,a}}+V_{\mathrm{act,c}}$$
$$=\frac{R_{\mathrm{g}}\cdot T}{F}\cdot\ln\left[\frac{J}{2J_{0,\mathrm{a}}}+\sqrt{\left(\frac{J}{2J_{0,\mathrm{a}}}\right)^2+1}\right]+\frac{R_{\mathrm{g}}\cdot T}{F}\cdot\ln\left[\frac{J}{2J_{0,\mathrm{c}}}+\sqrt{\left(\frac{J}{2J_{0,\mathrm{c}}}\right)^2+1}\right] \quad (9)$$

where $J_{0,\mathrm{a}}$ and $J_{0,\mathrm{c}}$ are the corresponding exchange current density of anode and cathode, which are closed associated with the electrode microstructure and the operating conditions.

$$J_{0,\mathrm{a}}=1.3448\times10^{10}\cdot\left(\frac{p_{\mathrm{H_2}}}{p_{\mathrm{ref}}}\right)\cdot\left(\frac{p_{\mathrm{H_2O}}}{p_{\mathrm{ref}}}\right)\cdot e^{-\frac{E_{\mathrm{act,a}}}{R_{\mathrm{g}}\cdot T}} \quad (10)$$

$$J_{0,c} = 2.051\times10^{9}\cdot\left(\frac{p_{O_2}}{p_{ref}}\right)^{0.25}\cdot e^{-\frac{E_{act,c}}{R_g\cdot T}} \tag{11}$$

where $E_{act,a}$ and $E_{act,c}$ are the activation energy of anode and cathode.

In fuel cell, ionic charge is much more difficult to transfer than electrons, and the resistance to charge transfer results in a loss of the fuel cell voltage, also known as the ohm loss. The SOFC ohmic overvoltage can be expressed as below [32].

$$V_{ohm} = 2.99\times10^{-11}\cdot J\cdot l_e\cdot e^{\frac{10300}{T}} \tag{12}$$

The concentration overvoltage appears mainly because of the rapid fuel consumption at large current density. The concentration overvoltage for the SOFC can be expressed as below [35].

$$\begin{aligned} V_{conc} &= V_{conc,a} + V_{conc,c} \\ &= \frac{R_g\cdot T}{2F}\cdot\ln\left(\frac{1+\frac{R_g\cdot T\cdot l_a\cdot J}{2F\cdot D_a^{eff}\cdot p_{H_2O}}}{1-\frac{R_g\cdot T\cdot l_a\cdot J}{2F\cdot D_a^{eff}\cdot p_{H_2}}}\right) + \frac{R_g\cdot T}{4F}\cdot\ln\left(\frac{p_{O_2}}{\frac{p_c}{\delta_{O_2}}-\left(\frac{p_c}{\delta_{O_2}}-p_{O_2}\right)\cdot e^{\frac{R_g\cdot T\cdot l_c\cdot J\cdot\delta_{O_2}}{4F\cdot D_c^{eff}\cdot p_c}}}\right) \end{aligned} \tag{13}$$

where, $D_a^{eff} = \frac{\varepsilon}{\xi}\cdot\frac{D_{H_2\text{-}H_2O}\cdot D_{H_2,k}}{D_{H_2\text{-}H_2O}+D_{H_2,k}}$ for the effective diffusion coefficient of anode and $D_c^{eff} = \frac{\varepsilon}{\xi}\cdot\frac{D_{O_2\text{-}N_2}\cdot D_{O_2,k}}{D_{O_2\text{-}N_2}+D_{O_2,k}}$ for the cathode; δ_{O_2} equals to $\frac{\frac{\varepsilon}{\xi}\cdot D_{O_2,k}}{D_c^{eff}+\frac{\varepsilon}{\xi}\cdot D_{O_2,k}}$; ε is the electrode porosity; θ is the electrode tortuosity; $D_{H_2\text{-}H_2O}$ stands for the binary diffusion coefficient of H_2 and H_2O, and $D_{O_2\text{-}N_2}$ for O_2 and N_2; $D_{H_2,k}$ and $D_{O_2,k}$ are Knudsen diffusion coefficient of H_2 and O_2, respectively. l_a and l_c stand for the anode and cathode thickness, respectively.

For the auxiliary devices such as compressor, the power consumption (P_{comp}) and the discharge temperature (T_{out}) can be obtained by Eq. (14) and (15) [44].

$$T_{out} = T_{in} + T_{in}\left(\gamma^{\frac{R_g}{C_p}}-1\right)\cdot\frac{1}{\eta_{ISC}\cdot\eta_{MEC}} \tag{14}$$

$$P_{\text{comp}} = \phi \cdot C_p \cdot T_{\text{in}} \left(\gamma^{\frac{R_g}{C_p}} - 1 \right) \cdot \frac{1}{\eta_{\text{ISC}} \cdot \eta_{\text{MEC}}} \tag{15}$$

where ϕ is the gas molar flow; C_p is the specific heat capacity; γ is the compression ratio; η_{ISC} and η_{MEC} stand for the isentropic and mechanical efficiency, respectively.

For the heat exchanger, the energy equation can be expressed as below.

$$\phi_{\text{hot}} C_{p,\text{hot}} (T_{\text{h}} - T_{\text{l}}) = \phi_{\text{cool}} C_{p,\text{cool}} (T_{\text{h}} - T_{\text{l}}) \tag{16}$$

where ϕ_{hot} and ϕ_{cool} are the molar flow of hot and cool fluid, respectively.

3.1.2. GP subsystem modeling

In the GP subsystem, the role of high-low temperature WGS reaction is to produce H_2 while the TSA unit based on MH is for H_2 purification. The WGS reaction and the corresponding equilibrium constant are expressed in Eqs. (3) and (6). Besides, the reaction rate of the WGS can be calculated in Eq. (17).

$$r = -k \cdot \exp(-\frac{E_{\text{act}}}{R_{\text{g}} T}) \cdot \left(p_{\text{CO}} \right)^{\alpha_{\text{CO}}} \cdot \left(p_{\text{H}_2\text{O}} \right)^{\alpha_{\text{H}_2\text{O}}} \tag{17}$$

where k is the frequency factor of catalyst; α_{CO} and $\alpha_{\text{H}_2\text{O}}$ are the partial pressure order for reactant CO and H_2O, respectively.

The working principle of TSA unit for H_2 purification is that the adsorption capacity of hydrogen on the adsorbent (such as $MmNi_{4.6}Al_{0.4}$) can be changed with the change of temperature, so that hydrogen can be adsorbed and desorbed when the temperature is changed, thereby achieving the purpose of hydrogen separation. The specific hydrogen purification reaction is illustrated as Eq. (18) [45].

$$\text{MmNi}_{4.6}\text{Al}_{0.4} + 3\text{H}_2 \leftrightarrow \text{MmNi}_{4.6}\text{Al}_{0.4}\text{H}_6 \quad \Delta H = -30.1\,\text{kJ/mol H}_2 \tag{18}$$

The corresponding reaction dynamics of the MH for H_2 desorption is shown in Eq. (19) [46], among which the equilibrium pressure is the function of temperature as expressed below [47]. C_d is the reaction rate constant for desorption. $\rho_{MH,sat}$ and $\rho_{MH,emp}$ are density of the saturated and empty MH, respectively.

$$\dot{m}_{H_2} = C_d \cdot \exp(-\frac{E_{act}}{R_g T}) \cdot \left(\frac{p_g - p_{eq}}{p_{eq}} \right) \cdot \left(\rho_{MH,sat} - \rho_{MH,emp} \right) \tag{19}$$

$$p_{eq} = f(\frac{H}{M}) \cdot \exp\left[\frac{\Delta H_{MH}}{R_g} \cdot \left(\frac{1}{T} - \frac{1}{T_{ref}} \right) \right] \tag{20}$$

$$f(\frac{H}{M}) = \sum_{n=0}^{9} \left[a_n \cdot \left(\frac{H}{M} \right)^n \right]$$
$$= 0.0075 + 15.2935 \cdot (\frac{H}{M}) - 34.577 \cdot (\frac{H}{M})^2 + 39.9926 \cdot (\frac{H}{M})^3 - 26.7998 \cdot (\frac{H}{M})^4 + 11.0397 \cdot (\frac{H}{M})^5$$
$$- 2.8416 \cdot (\frac{H}{M})^6 + 0.446 \cdot (\frac{H}{M})^7 - 0.0391 \cdot (\frac{H}{M})^8 + 0.0014 \cdot (\frac{H}{M})^9 \qquad \text{for absorption}$$

$$f(\frac{H}{M}) = \sum_{n=0}^{9} \left[a_n \cdot \left(\frac{H}{M} \right)^n \right]$$
$$= -1.465 + 19.190 \cdot (\frac{H}{M}) - 42.086 \cdot (\frac{H}{M})^2 + 49.087 \cdot (\frac{H}{M})^3 - 33.819 \cdot (\frac{H}{M})^4 - 14.437 \cdot (\frac{H}{M})^5$$
$$- 3.858 \cdot (\frac{H}{M})^6 + 0.627 \cdot (\frac{H}{M})^7 - 0.0567 \cdot (\frac{H}{M})^8 + 0.0021 \cdot (\frac{H}{M})^9 \qquad \text{for desorption}$$

3.1.3. PEMFC subsystem modeling

Similar to the SOFC, the electrochemical model of the PEMFC can be expressed also in Eq. (7). Herein, the reversible voltage E_N, activation overvoltage V_{act}, concentration overvoltage V_{conc}, and ohmic overvoltage V_{ohm} are written in the following equations [48].

$$E_{N,PEM} = 1.229 - 0.85 \times 10^{-3} \cdot (T - 298.15) + \frac{R_g \cdot T}{4F} \cdot \ln\left(p_{H_2}^2 \cdot p_{O_2} \right) \tag{21}$$

$$V_{act} = 0.948 - (0.00286 + 0.0002 \ln A + 4.3 \times 10^{-5} \cdot \ln \frac{p_{H_2}}{1.09 \times 10^6 \cdot e^{\frac{77}{T}}}) \cdot T$$
$$- 7.6 \times 10^{-5} \cdot T \cdot \ln \frac{p_{O_2}}{5.08 \times 10^6 \cdot e^{-\frac{498}{T}}} + 1.93 \times 10^{-4} \cdot T \cdot \ln I \tag{22}$$

$$V_{\text{ohm}} = I \cdot \left\{ \frac{181.6 \cdot \left[1 + 0.03 \cdot J + 0.062 \cdot \left(\frac{T}{303} \right)^2 \cdot J^{2.5} \right]}{\left(\psi - 0.634 - 3 \cdot J \cdot e^{4.18 \cdot \frac{T-303}{T}} \right)} \cdot \frac{l_e}{A} + 0.0003 \right\} \tag{23}$$

$$V_{\text{conc}} = -B \cdot \ln\left(1 - \frac{J}{J_{\max}} \right) \tag{24}$$

where A is the active cell area; I is the electric current; frequency factor of catalyst; ψ is adjustment parameter for humidity, herein $\psi = 14$ for the ideal humidity of 100%; l_e is the electrolyte thickness; B and $J_{\max}$ are the coefficient and the maximum current density, herein B=0.016 and $J_{\max}$=1.5 A/cm^2.

The FC output power P_{FC} can be obtained by Eq.(25), among which $\eta_{\text{DC/AC}}$ is the conversion efficiency of DC to AC.

$$P_{\text{FC}} = \eta_{\text{DC/AC}} \cdot J \cdot A \cdot V_{\text{cell}} \tag{25}$$

The gross and net electrical efficiency of the hybrid fuel cell power generation system can be defined as follows.

$$\eta_{\text{Gross}} = \frac{P_{\text{SOFC}} + P_{\text{PEM}}}{\phi_{\text{fuel}} \cdot LHV_{\text{fuel}}} \tag{26}$$

$$\eta_{\text{Net}} = \frac{P_{\text{SOFC}} + P_{\text{PEM}} - P_{\text{AUX}}}{\phi_{\text{fuel}} \cdot LHV_{\text{fuel}}} \tag{27}$$

The main parameters involved in the thermodynamic model of the proposed two-stage fuel cell hybrid system are shown in Table 1 [46,49–51].

Table 1. The meanings and values of the main parameters involved in the thermodynamic model.

Parameter	Value

SOFC operating temperature, T_{SOFC} (℃)	700~900
WGS operating temperature, T_{WGS} (℃)	160~380
TSA/PEMFC operating temperature, T_{PEM} (℃)	60~90
Operating pressure of the system, p (bar)	1.013
SOFC electrode porosity, ε	0.48
SOFC electrode tortuosity, ξ	5.4
SOFC anode thickness, l_a (mm)	1
SOFC cathode thickness, l_c (mm)	20×10^{-3}
Electrolyte thickness, l_e (mm)	8×10^{-3}
SOFC current density J_{SOFC}, (A/m^2)	6910
Activation energy of SOFC anode $E_{act,a,SOFC}$, (kJ/mol)	100
Activation energy of SOFC cathode $E_{act,c,SOFC}$, (kJ/mol)	120
Activation energy of HT-WGS $E_{act,WGS}$, (kJ/mol)	80.39
Activation energy of LT-WGS $E_{act,WGS}$, (kJ/mol)	78.29
Activation energy of TSA $E_{act,TSA}$, (kJ/mol)	23.88
Rate constant for desorption C_d, (s^{-1})	9.57
Frequency factor of catalyst of HT-WGS k_{HT}, (kmol/kg/s/bar)	108
Frequency factor of catalyst of LT-WGS k_{LT}, (kmol/kg/s/bar)	390
Partial pressure order for reactant CO of HT-WGS $\alpha_{CO,HT}$	0.58
Partial pressure order for reactant CO of LT-WGS $\alpha_{CO,LT}$	-0.14
Partial pressure order for reactant H_2O of HT-WGS $\alpha_{H_2O,HT}$	0.04
Partial pressure order for reactant H_2O of LT-WGS $\alpha_{H_2O,LT}$	0.62
PEMFC current density J_{PEM}, (A/m^2)	2500
DC/AC conversion efficiency, $\eta_{DC/AC}$	0.96

Isentropic efficiency of compressor, η_{ISC}	0.80
Mechanical efficiency of compressor, η_{MEC}	0.90

3.2. Thermo-economic modeling

This work employs a comprehensive thermo-economic index to assess the thermo-economic performance of proposed hybrid power generation system, which is the specific electric energy cost (SEEC) as expressed by Eq. (28) [52]. The total annual cost of the hybrid FC system includes six different annual fees, which are annual depreciation C_{Depr}, operation C_{Oper}, maintenance C_{Main}, investment interest C_{Int}, insurance C_{Ins} and tax C_{Tax}. Herein, the annual depreciation cost is the average allocation of all the component capital investment costs on the basis of life cycle $\lambda = 20$ year, as expressed in Eq. (29). Table 2 shows the capital cost estimation models of different components and the key parameters involved in the models.

$$SEEC = \frac{C_{Depr} + C_{Oper} + C_{Main} + C_{Int} + C_{Ins} + C_{Tax}}{(P_{SOFC} + P_{PEM}) \cdot t_{oper} / \lambda} \tag{28}$$

$$C_{Depr} = \frac{C_{Capi}}{\lambda} = \frac{C_{SOFC} + C_{WGS} + C_{TSA} + C_{PEM} + C_{Comp} + C_{HEX}}{\lambda} \tag{29}$$

Table 2. Capital cost estimation models of different components and the key parameters involved in the models

Capital cost	Capital cost equation	Value	Refs
C_{SOFC}	$C_{SOFC} = C_{Stack} + C_{AUX} + C_{INV}$		[36,53]

C_{PEM}	Stack cost: $C_{Stack} = A_{cell} \cdot \left(2.96 \cdot T_{SOFC} - 1907\right)$ Inverter cost: $C_{INV} = 10^5 \cdot \left(\frac{P_{SOFC}}{500}\right)^{0.70}$ Auxiliary devices cost: $C_{AUX} = 0.1 \cdot C_{Stack}$ $C_{PEM} = C_{Stack} + C_{AUX} + C_{INV}$ $C_{Stack} = b_1 \cdot \left[\left(\frac{b_2 - 105.4}{10} + 1437.3 \cdot L_{Pt} \cdot C_{Pt}\right) \cdot \frac{A_{cell} \cdot (1+\delta)^{\lambda}}{1000} + b_3\right]$ $C_{INV} = 10^5 \cdot \left(\frac{P_{PEM}}{500}\right)^{0.70}$ $C_{AUX} = c_1 + c_2 \cdot P_{PEM} - c_3 \cdot P_{PEM}^{\ 2}$	b_1=1.1; b_2=811.77; b_3=1311.3; δ =6%/year c_1=3343.5 USD; c_2=39.942 USD/kW; c_3=0.0454 USD/kW^2; Load amount of Pt: L_{Pt}=0.6 mg/cm^2; Price of Pt: C_{Pt}=0.0122 USD/mg	[54,55]
C_{WGS}	$C_{WGS} = C_{WGS\text{-}reac} + C_{WGS\text{-}cata}$ Reactor cost: $C_{WGS\text{-}reac} = C_{ref} \cdot \beta \cdot \left(\frac{W_{WGS}}{W_{ref}}\right)^{\gamma}$ Catalyst cost: $C_{WGS\text{-}cata} = W_{Cata} \cdot C_{Cata}$ $\beta = a_1 + a_2 \cdot \beta_m \cdot \beta_p$ $\beta_p = d_0 + d_1 \cdot \log(p) + d_2 \cdot \log(p)^2 + d_3 \cdot \log(p)^6 + d_4 \cdot \log(p)^8$ Reactor volume: $W_{WGS} = W_{factor} \cdot W_{Cata}$ Catalyst volume: $W_{Cata} = \frac{\phi_{in}}{\rho_{Cata}} \int_{X=0}^{X=X_r} \frac{dX}{-r}$	a_1=1.62; a_2=1.47; $\beta_m = 1$ d_0=0.5146; d_1=0.6838; d_2=0.297; d_3=0.0235; d_4=0.002; $\gamma = 0.59$ Reference volume: $W_{ref} = 0.104\ m^3$; Reference cost: $C_{ref} = 5774$ USD; Volume factor: $W_{factor} = 1.17$ Catalyst price: C_{Cata}= 100000 USD/m^3 Catalyst density: $\rho_{Cata} = 1200$ kg/m^3	[55–57]
C_{Comp}	$C_{comp} = 91562\left(P_{comp}/445\right)^{0.67}$		[58]
C_{HEX}	$C_{HEX} = 130 \cdot \left(\frac{A_{HEX}}{0.093}\right)^{0.78}$		[59]
C_{TSA}	$C_{TSA} = C_{MH} + C_{reac}$	H_2 capacity: ω_{MH} =1.39 wt%; MH price:	[60,61]

MH cost: $C_{\mathrm{MH}} = \dfrac{3600 \cdot \phi_{\mathrm{H_2}} \cdot t_{\mathrm{oper}}}{\chi_{\mathrm{MH}} \cdot n_{\mathrm{cycle}} \cdot t_{\mathrm{cycle}}} \cdot \omega_{\mathrm{MH}}$	χ_{MH} =36.91 USD/kg;
Reactor cost[a]: $C_{\mathrm{reac}} = W_{316\mathrm{L}} \cdot \rho_{316\mathrm{L}} \cdot C_{316\mathrm{L}}$	MH cycle life: n_{cycle} =18180;
	Each cycle time: t_{cycle} =3.333 h;
	316L density: ρ_{316L} =7980 kg/m^3;
	316L price: C_{316L} =3.287 USD/kg

a: The MH reactor is composed of stainless steel 316L

The annual operation fee C_{Oper}, depreciation fee C_{Dep}, maintenance fee C_{Main}, investment interest C_{Int}, insurance C_{Ins} and tax C_{Tax} are calculated by Eqs. (30-35), respectively.

$$C_{\mathrm{Oper}} = \phi_{\mathrm{fuel}} \cdot \chi_{\mathrm{fuel}} \cdot \frac{t_{\mathrm{oper}}}{\lambda} \tag{30}$$

$$C_{\mathrm{Dep}} = \frac{C_{\mathrm{Capi}}}{\lambda} \tag{31}$$

$$C_{\mathrm{Main}} = \frac{C_{\mathrm{Capi}}}{\lambda} \cdot f_{\mathrm{Main}} \tag{32}$$

$$C_{\mathrm{Int}} = \frac{C_{\mathrm{Capi}}}{\lambda} \cdot f_{\mathrm{Int}} \tag{33}$$

$$C_{\mathrm{Ins}} = \frac{C_{\mathrm{Capi}}}{\lambda} \cdot f_{\mathrm{Ins}} \tag{34}$$

$$C_{\mathrm{Tax}} = \frac{C_{\mathrm{Capi}}}{\lambda} \cdot f_{\mathrm{Tax}} \tag{35}$$

where $t_{\mathrm{oper}} = 8000$ h/year [37] is the operation time; ϕ_{fuel} and χ_{fuel} are the molar flow and price of the methanol fuel, respectively. Herein, the current methanol price $\chi_{\mathrm{fuel}} = 0.254$ \$/kg (Jan. 9th,

2020) of Northwest China is employed. $f_{\mathrm{Main}} = 0.06$, $f_{\mathrm{Int}} = 0.049$, $f_{\mathrm{Ins}} = 0.2$, and $f_{\mathrm{Tax}} = 0.06$ respectively stand for the corresponding factor.

4. Results and discussion

4.1. Model verification

The comparison between experiment and simulation on the component level instead of the system level is conducted for model validation, because no relevant experimental about this novel coupled high and low temperature fuel cell system for power generation is available in the existing literature. In the proposed hybrid system, the SOFC and PEMFC are the two main components and the electrochemical models are relative complex. Therefore, the model validation focuses on the SOFC and PEMFC components.

Fig. 2 displays the comparison between experimental data and simulation result of the voltage-current curves at different operating conditions. As shown in Fig. 2, the voltage-current curve predicted by SOFC model is in good agreement with the experimental result [62] of methanol-fed SOFC at different operating temperatures of 650~800 ℃. Besides, the good agreement between the simulation results using the proposed model and the experimental data [63] in different operating pressures of 1~5 bar is also observed in the hydrogen-fed PEMFC, as shown in Fig. 2b. The good agreements for both SOFC and PEMFC components well validate the established thermodynamic model of the SOFC-PEMFC hybrid system.

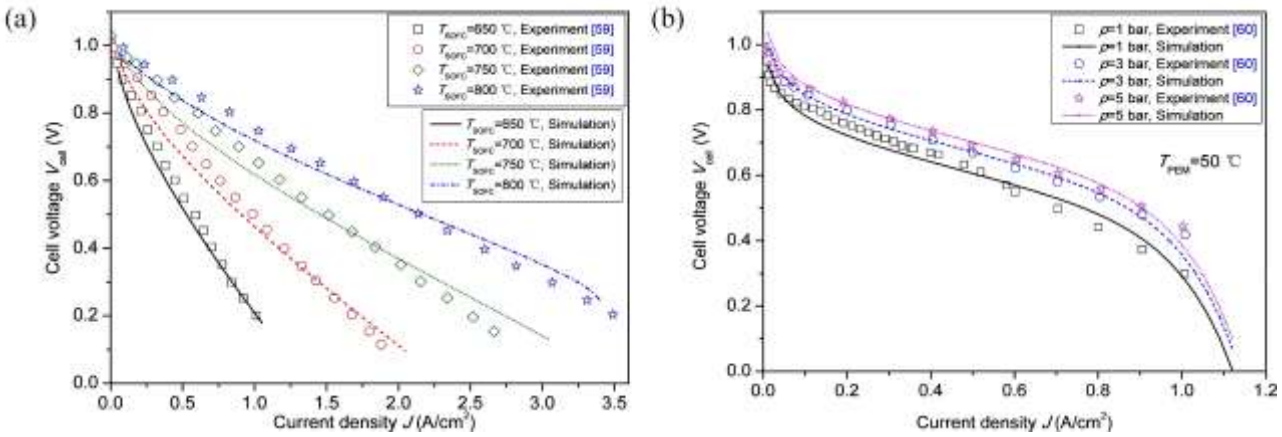

Fig. 2. The validation between experimental and simulation data for SOFC and PEMFC (a) SOFC at different operating temperatures of 650~800 ℃; (b) PEMFC in different operating pressures of 1~5 bar.

4.2. Thermodynamic evaluation of the hybrid system

As mentioned above, the fuel of PEMFC comes from the unconsumed fuel of SOFC off-gas in the SOFC-GP-PEMFC system. In other words, the power generation by the downstream PEMFC relies mainly on the degree of fuel consumption of the upstream SOFC. Generally, the parameters of recirculation ratio of SOFC anode off-gas and fuel utilization ratio are adopted to adjust the degree of fuel consumption for the SOFC. Therefore, this work first studied the impact of these two parameters on the energy conversion performance of this two-stage fuel cell system. Fig. 3a shows the component output power and energy efficiency of the hybrid system under different recirculation ratios. Herein, the operating conditions of this hybrid power system are set as T_{SOFC}=800 ℃, $T_{HT\text{-}WGS}$=350 ℃, $T_{LT\text{-}WGS}$=190 ℃, T_{TSA}=T_{PEM}=80 ℃, ϕ_{fuel} = 2.30 mol/s and μ=0.8. It can be seen that the gross efficiency of the whole system slightly increases when the recirculation ratio is increasing. On the contrary, both the overall and net electrical efficiency decrease. There are two main reasons for the reduced energy conversion efficiency at the higher recirculation ratio of SOFC anode off-gas. On the one hand, the higher recirculation ratio means more fresh fuel for the SOFC,

resulting in the increased SOFC power output. The SOFC power increases from 851 to 1013 kW, when the recirculation ratio is increased from 0 to 0.8, while the output power of downstream PEMFC is remarkably decreased from 187 to 45 kW. This is because more fuel consumed inside the SOFC subsystem resulting in the reduction of the fuel flow imported to PEMFC. Although the total output power of the system is slightly increased, the net power output is reduced with the increase of recirculation ratio. That is because the power consumption of auxiliary devices (compressor 1 and compressor 2) is also increased at the high recirculation ratio. Especially for the compressor 1, the required power is significantly increased due to more air supply for more fuel consumption in electrochemical reaction inside the SOFC. From Eq. (15), the power consumption of the compressor increases linearly with the increase of the inlet gas flow. It was found that the auxiliary power consumption is increased from 141 to 204 kW with the recirculation ratio increasing from 0 to 0.8. Therefore, the reduced net power causes the lower net electrical efficiency for the hybrid power system at a higher recirculation ratio. On the other hand, the less H_2 production suggests the smaller reaction heat is required for the MH-based TSA to supply H_2 for the PEMFC. Accordingly, the thermal efficiency is smaller due to the less waste heat recovery, resulting in the lower overall efficiency at the higher recirculation ratio. Herein, it is worth noting that the power distribution between SOFC and PEMFC also becomes more imbalanced at the higher recirculation ratio, which is nearly 96:4 at the recirculation ratio of 0.8 as shown in Fig. 3b. Therefore, in consideration of efficiency improvement and power balance, no SOFC anode off-gas recirculation is recommended for the two-stage hybrid FC power generation system.

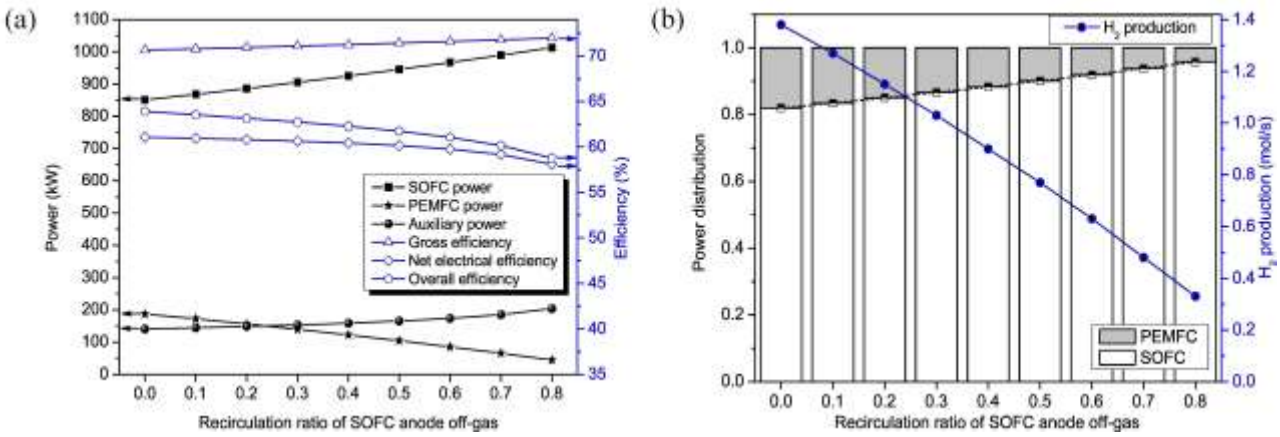

Fig. 3. The effect of recirculation ratio of SOFC anode off-gas on the performance of the hybrid system (a) Power and efficiency; (b) Power distribution and H_2 production.

The effect of SOFC fuel utilization ratio μ on the performance of the hybrid power system with no recirculation ratio for the SOFC anode is shown in Fig. 4. Clearly, the variation trend of the power output and energy efficiency caused by SOFC fuel utilization ratio is almost the same as the case of above-mentioned recirculation ratio. The difference is that the fuel utilization ratio has a larger impact than the recirculation ratio. For example, the SOFC power varies from 106 to 957 kW at different fuel utilization ratios, while the variation range of SOFC power with different recirculation ratios is 851~1013 kW. By adjusting the SOFC fuel utilization, the power output of the PEMFC varies significantly from 90 up to 850 kW. Accordingly, the power distribution between SOFC and PEMFC can be reasonably controlled through fuel utilization ratio, which can vary from 11% to 91% for the SOFC power ratio. As the fuel utilization ratio of SOFC is set about 0.5, the power distribution becomes balanceable as shown in Fig. 4b. In such case, the gross and net electrical efficiency of the whole system are 68.0% and 61.6%, respectively.

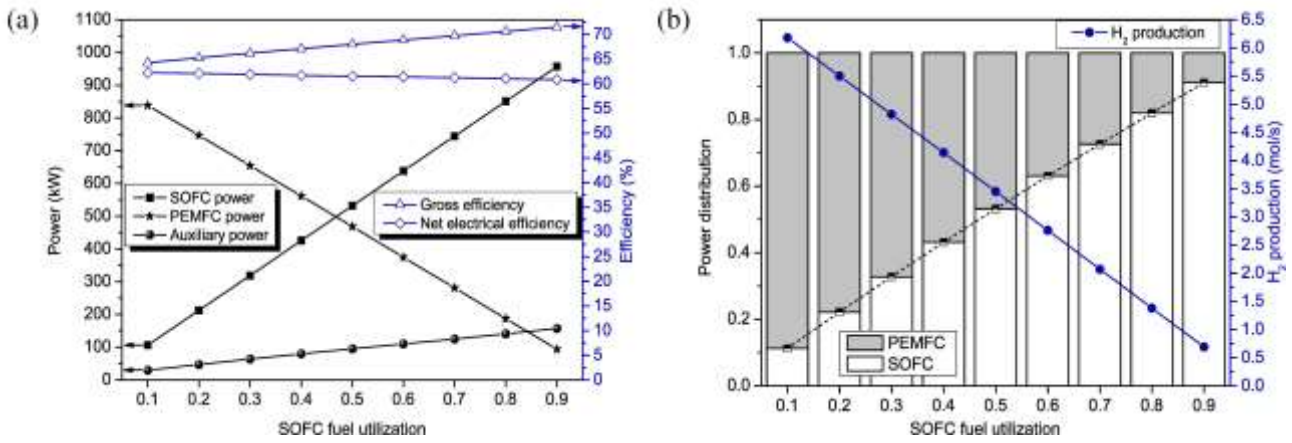

Fig. 4. The effect of SOFC fuel utilization ratio on hybrid system performance (a) Power and efficiency; (b) Power distribution and H_2 production.

Besides the SOFC fuel utilization ratio and recirculation ratio, the operating temperature is another key parameter that affects SOFC performance. As the operating temperature of SOFC rises from 700 to 900 ℃, the SOFC output power is accordingly increased from 415 to 588 kW as shown in Fig. 5a. This is mainly because of the smaller polarization overvoltage at the higher temperature, which leads to the higher cell voltage and increased power output for the SOFC under the same current density. In contrast to the SOFC, the PEMFC and auxiliary power slightly reduce. The main reason is that the amount of H_2 composition in the anode off-gas changes a little at high operating temperatures, which varies in a very small range of 3.44~3.45 mol/s. In fact, the gas composition of the SOFC anode exhaust is primarily determined by the WGS equilibrium, as the MD and MSR reactions taking place within the SOFC are close to completion [38]. Since WGS reaction is a reversible exothermic reaction, it will move in the opposite direction with the increase of temperature, resulting in a decrease in hydrogen production, which also makes the PEMFC power slightly reduce at the elevated SOFC operating temperature. However, due to a large increase in SOFC output power, the total net output power of whole system increases as the improvement of

SOFC temperature. Accordingly, the gross and net electrical efficiency of the hybrid power system increase from approximately 60% to 72% and from about 52% to 66%, respectively. Although the high SOFC operating temperature helps to increase the energy conversion efficiency and thus decrease slightly the SEEC of the hybrid FC power generation system. However, this improvement of energy efficiency is at the expense of increasing the SOFC component cost as shown in Fig. 5b. Since the SOFC is a high-temperature component, its capital cost depends to some extent on the operating temperature according to the SOFC capital cost model listed in Table 2. When the temperature increases from 700 to 900 ℃, the capital cost of SOFC component is greatly increased from 1.3 to 2.0 million CNY. Besides, the SOFC cost ratio in the hybrid system is increased up to approximately 19% accordingly. Therefore, the moderate operating temperature of about 800 ℃ is employed for the SOFC in the following analysis.

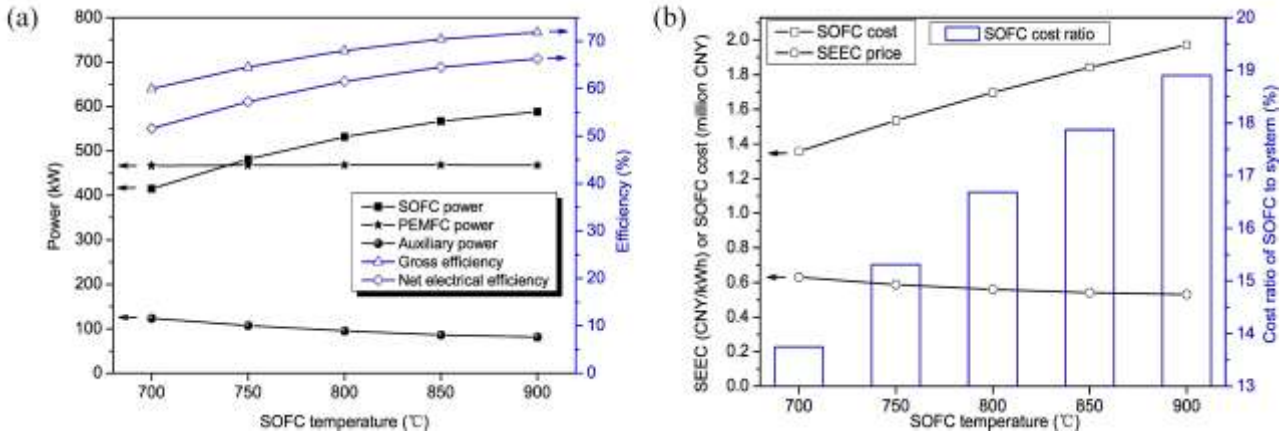

Fig. 5. The effect of SOFC operating temperature on the performance of the hybrid power system (a) Thermodynamics; (b) Thermo-economics.

In order to increase the hydrogen flow into the PEMFC, the WGS reaction is coupled to convert the CO from the SOFC off-gas into H_2. Generally, the H_2 production mainly depends on the operating temperature of WGS, which determines the reaction equilibrium constant. Fig. 6 displays

the impacts of HT- and LT-WGS operating temperatures on the thermodynamic and thermo-economic performance of the whole system. Herein, the HT-WGS temperature varies from 320 to 380 ℃, while the range of 160~220 ℃ is for the LT-WGS. The role of the HT-WGS is to speed up the H_2 conversion rate. Actually the high temperature has little influence on the amount of H_2 production due to the exothermic reaction of WGS. As a result, the power generation by PEMFC remains almost unchanged at different HT-WGS temperatures. By contrast, the temperature of LT-WGS has a greater influence on H_2 conversion rate, whose main role is to increase H_2 production for the PEMFC as listed in Table 3. As seen in Fig. 6b, the PEMFC power and net electrical efficiency are increased with the reduction of the LT-WGS temperature. Moreover, it was found that the CO concentration of the exhaust gas of LT-WGS can be controlled below 0.1% when the LT-WGS temperature is lower than 200 ℃. It was reported that the maximum concentration of CO impurity for not poisoning the AB_5-type MH used in this work must be below 0.1% [64]. Therefore, the control of LT-WGS reaction temperature below 200 ℃ is essential to prevent the follow-up TSA process for H_2 purification from being poisoned by CO. However, the lower tempreature usually results in the larger WGS capital cost, whose ratio in the hybrid system is increased from 5% to 12% with the decrease of tempreature from 220 to 160 ℃. Anyway, the operating temprature of WGS unit has little impact on system SEEC because the cost of WGS unit account for a small percentage of the total cost of the hybrid system.

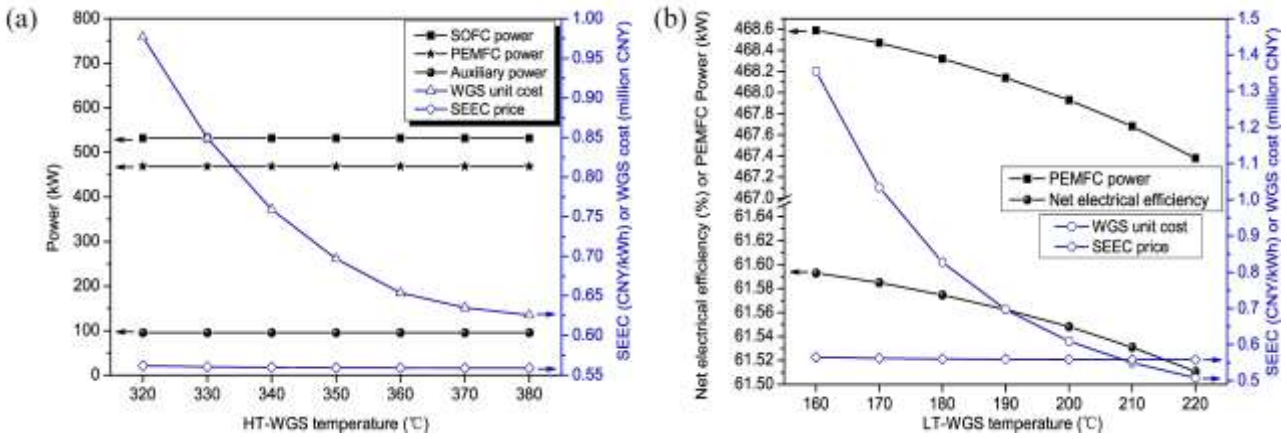

Fig. 6. The effect of two-stage WGS temperatures on the system thermodynamic and thermo-economic performance (a) HT-WGS; (b) LT-WGS.

Table 3. The CO and H_2 concentration of the exhaust gas from LT-WGS component at different operating temperatures.

Concentration	LT-WGS operating temperature (℃)						
	160	170	180	190	200	210	220
CO	0.03%	0.04%	0.05%	0.06%	0.08%	0.10%	0.12%
H_2	34.05%	34.04%	34.03%	34.02%	34.01%	33.99%	33.97%

As described above in Fig. 1, the role of TSA unit aims at the H_2 purification and supply for the downstream PEMFC. Herein, the AB_5-type metal hydride is used as the hydrogen purification medium of TSA unit for reversible H_2 absorption and desorption by chemical reaction. Actually, the PEMFC operating temperature can be self-regulated by the TSA operating temperature, indicating almost the same temperature for the PEMFC and TSA reactor. Fig. 7 illustrates the system power, efficiency and SEEC trends under TSA or PEMFC operating temperatures of 60~90 ℃. With the increase of the temperature, the power output of PEMFC is also increased from 458 to 472 kW.

Accordingly, the net electrical efficiency of the system is increased up to about 62%, which is because the amount of H_2 released from TSA reactor is increased at the higher temperature according to Eq. (19). In addition, the SEEC is also reduced from 0.5650 to 0.5568 CNY/kWh for the hybrid system when the temperature is various from 60 to 90 ℃. It is of importance to note that the capital cost of PEMFC component is slightly increased at the higher temperature.

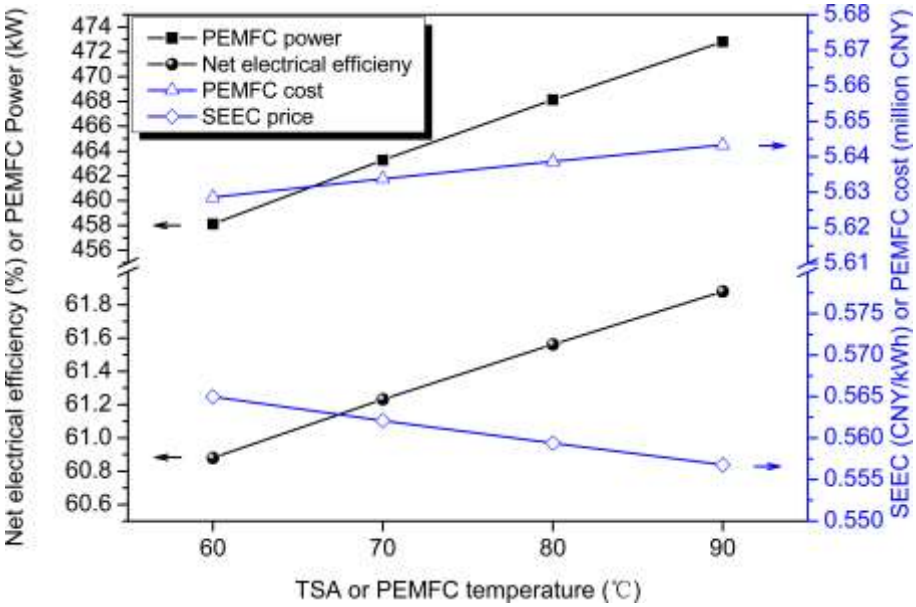

Fig. 7. The effect of TSA or PEMFC temperature on the PEMFC power, system efficiency and SEEC.

4.3. Thermo-economic evaluation of the hybrid power system

Thermo-economic evaluation of the proposed SOFC-GP-PEMFC system is further conducted. Fig. 8 shows the component costs and annual fees of the hybrid system. The PEMFC component accounts for more than half of the total capital cost. SOFC is the second largest capital cost component, which is 16.68%. Therefore, the most of the capital investment cost in hybrid system come from the contribution of two power generation components. The unit power generation cost of SOFC and PEMFC is calculated to be approximately 500 and 1700 USD/kW, respectively. Except

the electricity generation components, the TSA and WGS components for the gas processing also contribute to nearly 20%. For the hybrid power system, the annual fee includes the six kinds of different fees described by Eqs (30)-(35). Apparently, the operation fee dominates the annual fee, whose proportion is up to approximately 85% due to a high methanol consumption in the hybrid system. Except the operation fee, the depreciation fee also contributes to about 11%, which is the average allocation of the investment capital cost actually.

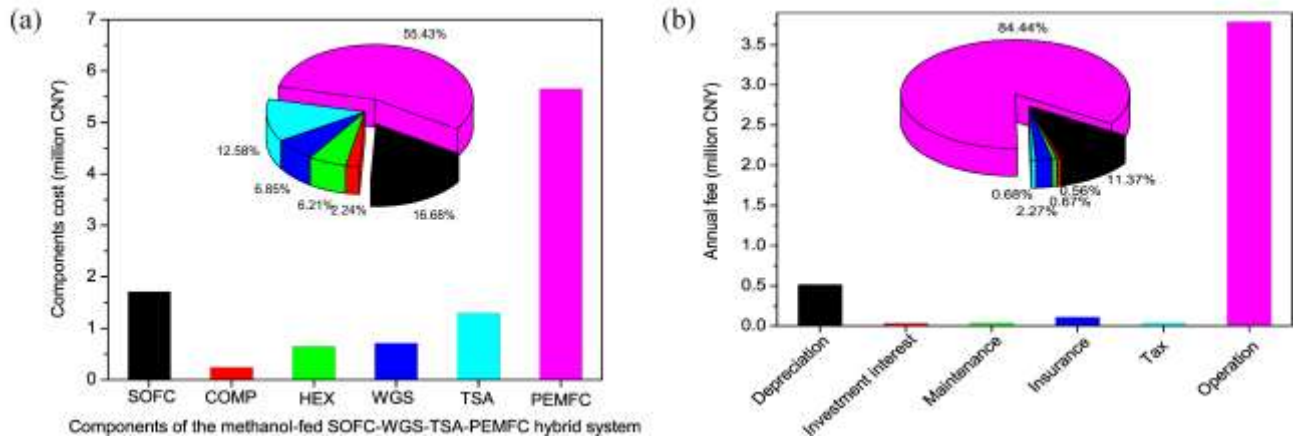

Fig. 8. The component costs and annual fees of the hybrid system (a) Component costs; (b) Annual fees.

The sensitivity analysis on the SEEC and annual fee of the hybrid fuel cell power system is depicted as Fig. 9. The influences of prices of 316L steel (the material for the reactors), MH, methanol fuel, WGS and PEMFC catalyst, insurance fee, maintenance fee and interest fee on SEEC are taken into account. Apparently, the SEEC of the hybrid power system is the most sensitive to the price fluctuation of methanol fuel among these market price factors, as shown in Fig. 9a. When methanol fuel price rises by 20%, the SEEC is also increased by 16.87%. Accordingly, the annual fee reaches up to 5.23 million CNY, as shown in Fig. 9b. The ratio of the SEEC incremental percentage to the percentage increase of fuel prices is defined as the sensitivity factor of the SEEC to methanol

price. This sensitivity factor was calculated to be about 0.8. Except the fuel price, the SEEC of the proposed hybrid system is less affected by the fluctuation of other market price factors. When the market price have a variation of 20%, the maximum fluctuation of the SEEC is no more than 0.5%. Therefore, the SOFC-GP-PEMFC hybrid power system presented in this work shows strong resistance to the price fluctuation of main market factors in the practical applications.

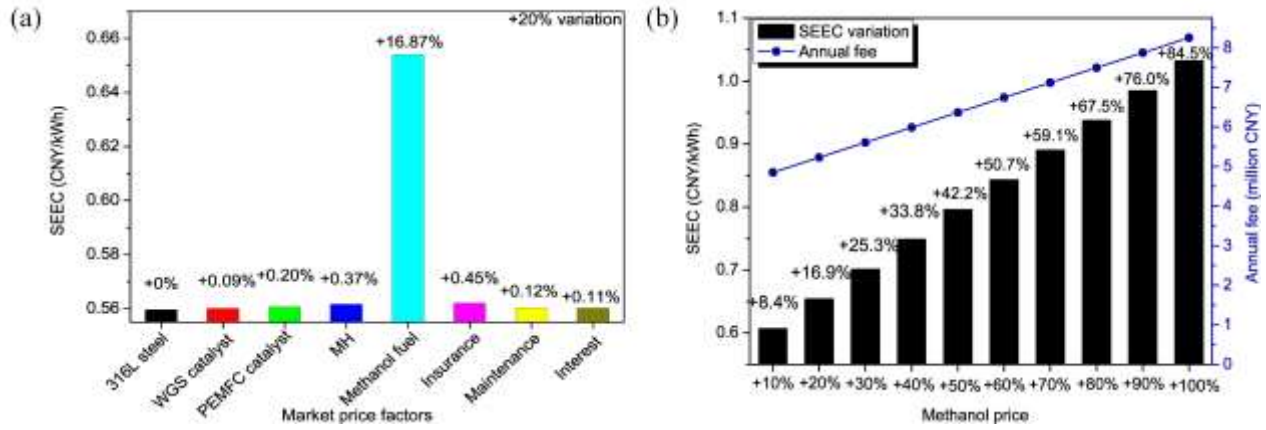

Fig. 9. The sensitivity analysis on thermo-economics of the hybrid power system (a) SEEC under the variation of 20% of main market price factors; (b) SEEC and annual fee under different methanol fuel prices.

4.4. Techno-economic benefits of the hybrid power system

From the thermodynamic and thermo-economic analyses, the optimal performance of the 1 MWe two-stage fuel cell hybrid power generation system fueled by methanol can be obtained, which is summarized in Table 4. Herein, the estimation of the SEEC of the present system is based on the current methanol price 0.254 USD/kg of Northwest China as fuel price. It can be seen that the SOFC and PEMFC component for electricity generation have comparable power output when the methanol mass flux is set as 0.07371 kg/s, which are 532 and 468 kW, respectively. The gross electrical efficiency of the proposed system is 68.03%. Excluding the power consumption of auxiliary

equipment, the net electrical efficiency of the system is 61.56%. In such power scale, the SEEC is 0.5594 CNY/kWh for the proposed hybrid power system, which is much lower than the power generation cost of the previously reported methanol power plants, such as 0.706 USD/kWh (about 5 CNY/kWh including the delivery cost) of the methanol power plant with 3300 MWh capacity used in northern remote communities of Canada [28], and 0.34 USD/kWh (2.4 CNY/kWh) of the methanol-fed MSR-PEMFC power plant [19].

Table 4. The energy and economic performance of the 1 MWe methanol-fed SOFC-GP-PEMFC hybrid system for power generation.

Parameters	Methanol flux (kg/s)	Power (kW)		Auxiliary power (kW)	Efficiency (%)		SEEC (CNY/kWh)
		SOFC	PEMFC		Gross	Net	
Values	0.07371	531.86	468.14	95.07	68.03	61.56	0.5594

Generally, the current methanol utilization methods for power generation mainly contain the standalone DMFC, SOFC, MTST, SI engine and the hybrid energy conversion systems of MSR-PEMFC, MSR-HTPEMFC, MSR-PEMFC-mCCHP, and SOFC-mGT. This work also compared the energy conversion efficiency of the proposed methanol utilization method with the other reported methanol utilization technologies and traditional coal fired power plant (CFPP), as shown in Fig. 10. Among the standalone energy systems, the SI engine has the lowest efficiency of 25% [7], while the methanol-fed SOFC has the highest efficiency of 50% [27,28]. Compared with the standalone system, the hybrid energy system usually presents a higher energy conversion efficiency. For example, the PEMFC-based and SOFC-based hybrid power systems were reported to have the largest efficiency of about 66% for the MSR-PEMFC-mCCHP [29] and 68% for the

SOFC-mGT [30], respectively. Our work combines the high-efficiency SOFC and PEMFC to form the hybrid power system. The energy conversion efficiency of the proposed system is 68.6% (including thermal efficiency of 7%), which is higher than those of the previously reported standalone and hybrid energy systems fed by methanol. Besides, the methanol-fed SOFC-GP-PEMFC hybrid power system as power plant is also more efficient than the traditional power plant of CFPP or CFPP-MCFC, whose energy conversion efficiency is about 35.9%~40% [65]. Actually, Guangdong Hejide Energy Technology Co., Ltd. has successfully developed and commercialized an efficient methanol-fed MSR-PEMFC power system called as 'AH7500 AH power module'. One of the product advantages is a high power generation efficiency of 1 kg methanol generating about 2.2 kWh, which is more than twice as high as that of traditional generators [66]. By comparison, the proposed SOFC-GP-PEMFC hybrid power system can generate about 3.2 kWh with 1 kg methanol. The comparison result confirms that the proposed methanol fueled SOFC-GP-PEMFC hybrid system is kind of high-efficiency energy conversion technology.

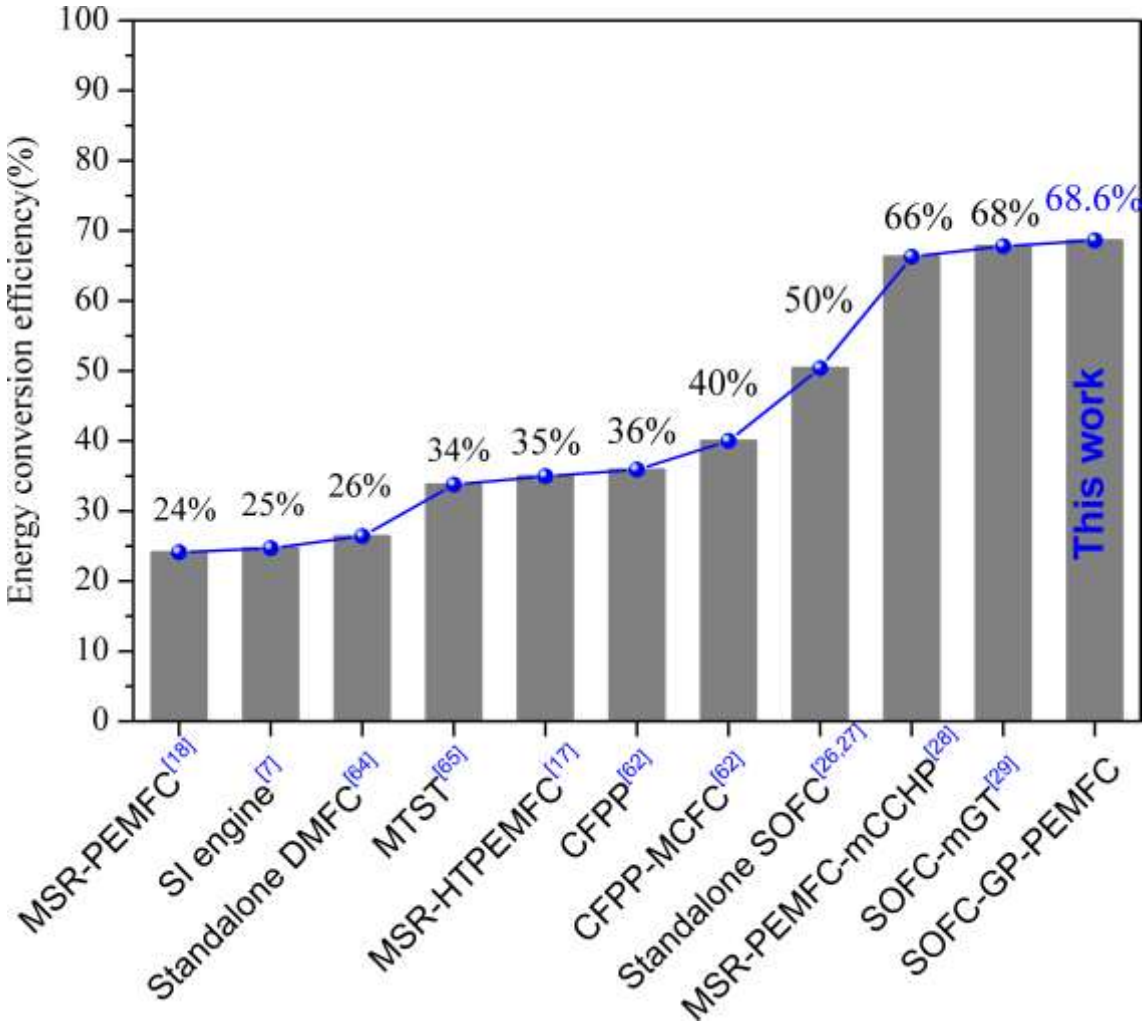

Fig. 10. The comparison of energy conversion efficiency between different methanol-fed energy systems and traditional coal fired technologies for power generation [7,18,19,27–30,65,67,68].

The exergy flow and the corresponding exergy analysis about the 1 MW methanol fueled the two-stage fuel cell hybrid system are further investigated. Fig. 11 illustrates Sankey diagram of exergy flow within the hybrid system. In the Sankey diagram, the thickness of the flow lines represents the amount of exergy flow, which can apparently visualize the exergy flow and exergy loss of an energy system. It can be seen that a large amount of exergy flow appears in the SOFC subsystem (upper diagram) due to the super-high operating temperatures over 700 ℃. By contrast, the GP and PEMFC subsystems (lower diagram) have a relatively smaller exergy flow. Among all

the components, the PEMFC has the largest exergy loss (322.1 kW) and has a relative exergy destruction of 33%. The TSA unit takes the second position, which has the exergy loss of 88.6 kW and the relative exergy loss of 9%. For the SOFC component, the exergy loss is only 57 kW, indicating that most of the energy inside the SOFC is available under a high temperature circumstances. Therefore, the system has a relative high exergy efficiency of 60.8%.

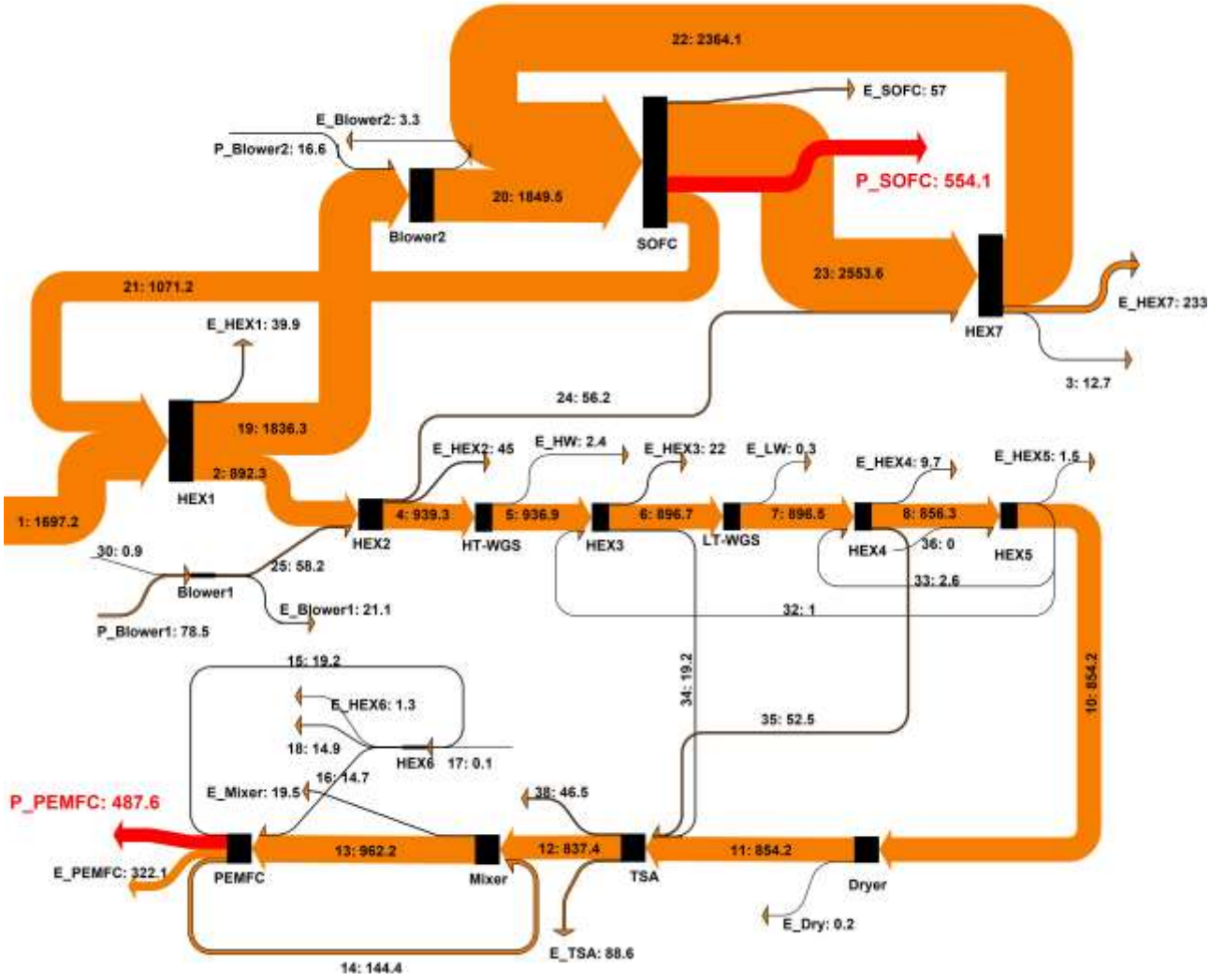

Fig. 11. Sankey diagram of the exergy flow within the 1 MWe methanol-fed hybrid system.

From the above-mentioned analyses, the proposed SOFC-GP-PEMFC hybrid power system exhibits the promising potential for the practical application due to its high energy and exergy efficiency. It is well known that the power scale is an important parameter for the energy system in

the application. Fig. 12a displays the effect of power scale (1~50 MWe) on system efficiency and SEEC. With the increase of system output power from 1 MWe to 50 MWe, the SEEC reduces gradually from 0.5594 to 0.5116 CNY/kWh. Besides, the overall energy conversion efficiency of this hybrid system remains almost unchanged. Therefore, large-scale for the hybrid systems is beneficial to decrease the SEEC during the power generation process.

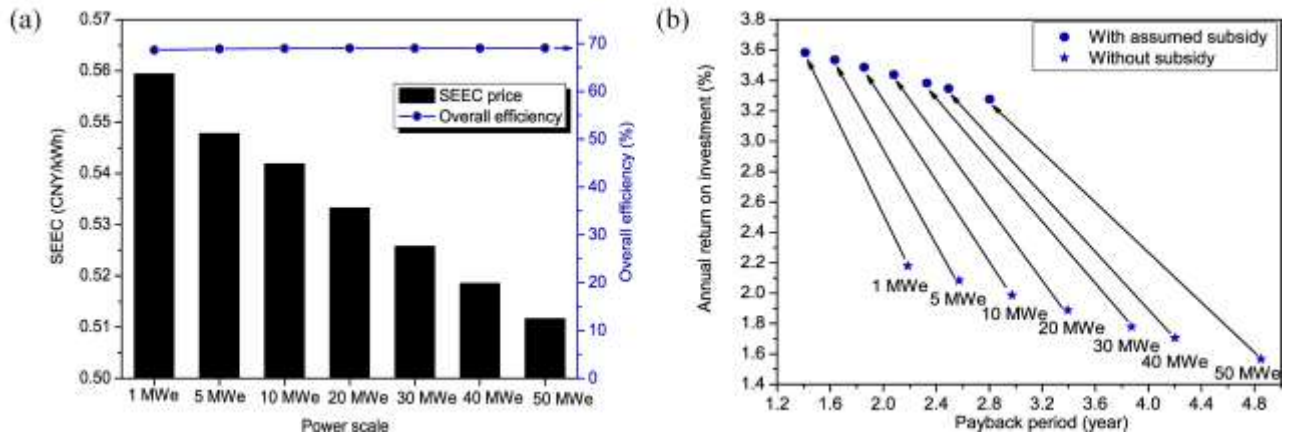

Fig. 12. The performance of the hybrid power system under different power scales and subsidies (a) The effect of power scale on SEEC and overall efficiency; (b) The effect of subsidy on annual return on investment and payback period.

As shown in Fig. 12b, with the increase of power scale, the technical-economic benefits of this hybrid system decrease negatively. Herein, this work employs the current electricity price for industry and commerce of Shaanxi province region of northwest China as the selling price of the generated electricity, which is 0.7346 CNY/kWh. With the increase of power scale from 1 to 50 MWe, the payback period is increased from 2.2 to 4.8 year and the annual return on investment is reduced from 2.18% to 1.57%. This is because that the larger power scale generally indicates the more capital investment to expand the power capacity. Additionally, the more methanol fuel is required for the larger power capacity, which causes the significant increase of operation fee. As

mentioned above in Fig. 8b, the operation fee and capital investment (allocated into depreciation fee) contribute to more than 95% of hybrid system annual fee. In consequence, the techno-economic benefits become worse at the large power scale, even though large-scale applications help reduce the SEEC of the hybrid system.

Although the methanol-fed SOFC-GP-PEMFC hybrid system has a relative high efficiency for clean electricity production, the cost of electricity generation is still high due to no mass production of fuel cell. Actually, the break even energy cost of a standard power plant was reported to be 0.0546 USD/kW h (0.383 CNY/kWh) [69], which is lower than the SEEC (0.5116~0.5594) of the methanol-fed hybrid power system. In China, the traditional coal fired power plant still dominates the electricity market. Recently, National Development and Reform Commission (NDRC) of China has just issued a new market-based price mechanism about the on-grid price of coal fired power generation instead of benchmark feed-in tariff at the beginning of 2020. The new price mechanism uses the current benchmark feed-in tariff as the standard price and allows the fluctuation in the range of no more than 10% floating upward and no more than 15% floating downward on the basis of standard price [70]. Statistically, 18 provinces and cities of China have employed the newly issued market-based price mechanism for the on-grid price of coal fired power plant until now, which is summarized in Fig. 13. The standard price is within the range of 0.2595~0.453 CNY/kWh for these regions, among which the region of South China has the largest on-grid price (0.4983 CNY/kWh in Guangdong province) and the lowest on-grid price (0.2206 CNY/kWh in Ningxia province) in Northwest China. The largest on-grid price of coal fired power plant in Guangdong region is mainly attributed to the large demand of electricity capacity but scarce coal resource. By contrast, the

Ningxia region with the lowest price has abundant coal resource and the power demand is not so large due to the relative backwardness in the local economy. Besides the region of South China, the region of East China also has the high standard electricity price of 0.3844~0.4155 CNY/kWh. Therefore, it can be concluded that the coal fired power plant is still cost-optimal for power generation in China. By comparison, the SEEC (0.5116~0.5594 CNY/kWh) of the methanol-fed SOFC-GP-PEMFC hybrid system is higher than the on-grid price (0.2206~0.4983 CNY/kWh) of the coal fired power plant.

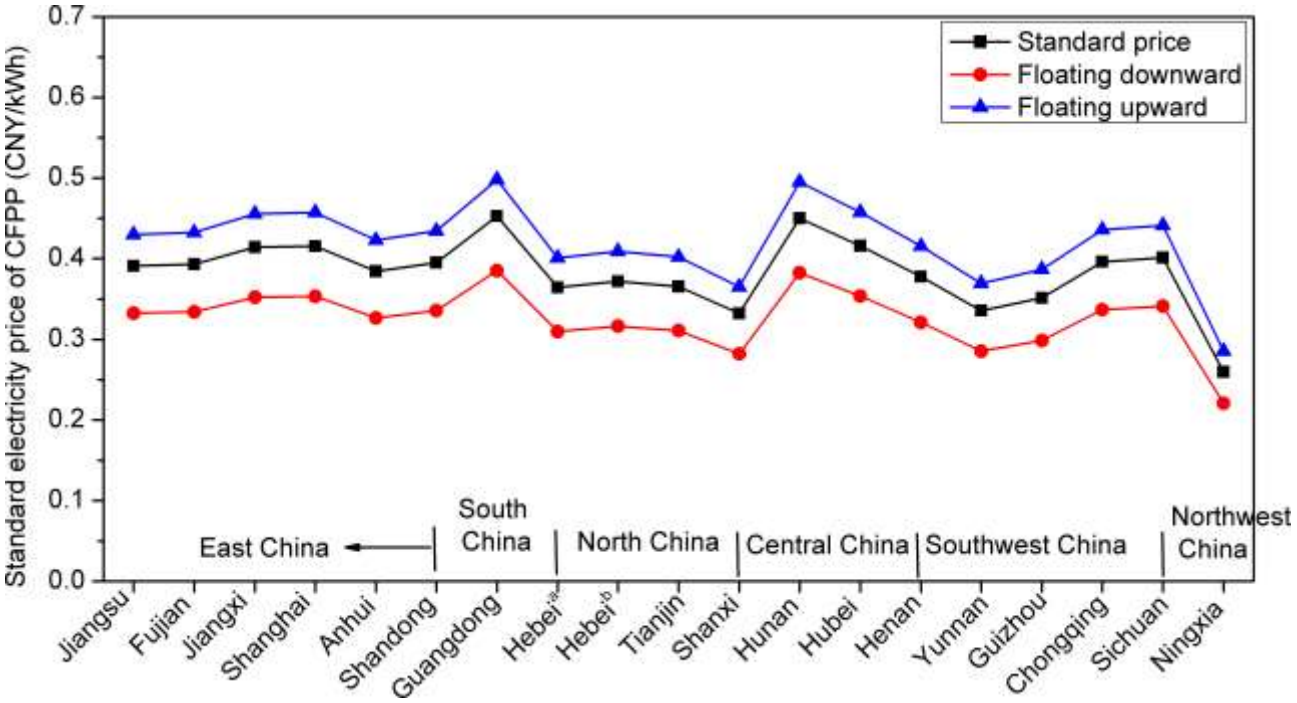

a: Southern Hebei Power Network
b: Northern Hebei Power Network

Fig. 13. The current standard electricity price and the corresponding floating range of the coal fired power plant in different regions of China.

However, many countries and regions plan to develop renewable energy resources, such as wind, solar, and biogas, for clean electricity power generation to partially replace the traditional CFPP. In order to encourage the clean power generation, financial subsidy is usually a must.

Actually, many countries and regions have put forward the financial subsidy to accelerate the development of novel clean power generation technology. For example, the NDRC, China subsidizes the renewable energy power plant by financially supporting the exceeding electricity price beyond the local benchmark feed-in tariff through renewable energy development fund. If the methanol power plant based on the proposed SOFC-GP-PEMFC hybrid technology is also supported by the government with the same subsidy level, the techno-economic benefits will be significantly increased. Taking Shaanxi province (Northwest region), China with the current benchmark feed-in tariff of 0.3345 CNY/kWh as our case, the payback period and annual return on investment of the methanol-fed hybrid power plant under different power scales of 1~50 MWe are compared in Fig. 12b. It can be seen that the payback period can be shortened to 1.4~2.8 year and the annual return on investment can be increased to 3.28~3.58% owing to the assumed subsidy level. The techno-economic benefits are more significant for the hybrid power system with smaller power capacity. As the power scale increases from 1 to 50 MWe, the subsidy level is also increased from 1.5 to 57 million CNY. Therefore, the methanol-fed hybrid power plant with small power capacity is preferentially encouraged in such subsidy policy. Besides, this kind of methanol power generation technology is more competitive in the regions of South China and East China because of the high on-grid electricity price in these regions.

5. Conclusions

A novel methanol utilization approach for power generation based on the SOFC-GP-PEMFC hybrid system was proposed in present work. The thermodynamic analysis is applied to this hybrid system for acquiring the basic operation data firstly. Then the evaluation including thermo-economic

and techno-economic analyses base the Northwest China, was further performed to reveal the potential feasibility of the methanol power plant in the practical applications. Through the 3T evaluation, several conclusions can be drawn as follows.

(1) In consideration of improved efficiency and balanceable power distribution between SOFC and PEMFC, the strategy of no recirculation ratio of anode off-gas and moderate fuel utilization of about 0.5 are recommended for the operation of SOFC. After the performance optimization, the overall efficiency reaches up to 68.6%, which is higher than those of the previously reported standalone and hybrid energy systems fed by methanol as well as traditional coal fired power plant, such as standalone DMFC, SOFC, SI engine, MSR-PEMFC-mCHPP, CFPP-MCFC, and SOFC-mGT.

(2) The operating temperature of the LT-WGS should be controlled below 200 ℃ to ensure the CO concentration of the exhaust gas less than 0.1%, thus to preventing the TSA working medium MH being poisoned in the H_2 purification process.

(3) The SEEC of 1 MWe methanol-fed hybrid power system is 0.5594 CNY/kWh, which is much lower than the power generation cost of the previously reported methanol power plants, such as MSR-PEMFC. As the power scale increases to 50 MWe, the SEEC further reduces to 0.5116 CNY/kWh. Therefore, large-scale has the promotion effect to reduce the system power generation cost.

(4) The electricity production cost (0.5116~0.5594 CNY/kWh) of the methanol power plant is still higher than the present on-grid price (0.2206~0.4983 CNY/kWh) of the traditional coal fired power plant in China. However, with the current financial subsidy level for encouraging

renewable energy power plant, the payback period can be shorten to 1.4 year and the annual return on investment can be increased to 3.58%.

(5) This kind of methanol power plant with small power capacity (~1 MWe) is preferentially encouraged to develop in the regions of South China and East China because of the high on-grid electricity price and scarce coal resource in these regions.

Acknowledgments

Z. Wu thanks the funding support from the Natural Science Foundation of Shaanxi Province (No. 2020JM-014), China-Central Eastern European Countries Higher Education Institutions Consortium (No. 202006) and Hong Kong Scholar Program (No. XJ2017023). M. Ni thanks the funding support (Project Number: PolyU 152214/17E and PolyU 152064/18E) from Research Grant Council, University Grants Committee, Hong Kong SAR.

References

[1] Khirennas A, Talha A, Kaabeche A, Bakelli Y, Overview of fossil fuel-based hybrid power generation systems within mini-grids – The experience of storage-less PV system integration into three of the Great Algerian South mini-grids. Energy Conversion and Management 2020;221, article 113191. doi.org/10.1016/j.enconman.2020.113191.

[2] Lin BQ, Ouyang XL. A revisit of fossil-fuel subsidies in China: Challenges and opportunities for energy price reform. Energy Conversion and Management 2014;82:124-134. doi.org/10.1016/j.enconman.2014.03.030.

[3] Yan H, Wang G, Lu Z, Tan P, Kwan TH, Xu H, et al. Techno-economic evaluation and technology roadmap of the MWe-scale SOFC-PEMFC hybrid fuel cell system for clean power generation. J Clean Prod 2020;255:120225. doi:10.1016/j.jclepro.2020.120225.

[4] Ni M. 2D thermal modeling of a solid oxide electrolyzer cell (SOEC) for syngas production by H2O/CO2 co-electrolysis. Int J Hydrogen Energy 2012;37:6389–99. doi:10.1016/j.ijhydene.2012.01.072.

[5] Olah GA. Beyond Oil and Gas: The Methanol Economy. Angew Chemie Int Ed 2005;44:2636–9. doi:10.1002/anie.200462121.

[6] Yao Y, Chang Y, Huang R, Zhang L, Masanet E. Environmental implications of the methanol economy in China: well-to-wheel comparison of energy and environmental emissions for different methanol fuel production pathways. J Clean Prod 2018;172:1381–90. doi:10.1016/j.jclepro.2017.10.232.

[7] Wu B, Wang L, Shen X, Yan R, Dong P. Comparison of lean burn characteristics of an SI engine fueled with methanol and gasoline under idle condition. Appl Therm Eng 2016;95:264–70. doi:10.1016/j.applthermaleng.2015.11.029.

[8] Gong C, Li Z, Chen Y, Liu J, Liu F, Han Y. Influence of ignition timing on combustion and emissions of a spark-ignition methanol engine with added hydrogen under lean-burn conditions. Fuel 2019;235:227–38. doi:10.1016/j.fuel.2018.07.097.

[9] Nidhi, Subramanian KA. Experimental investigation on effects of oxygen enriched air on performance, combustion and emission characteristics of a methanol fuelled spark ignition engine. Appl Therm Eng 2019;147:501–8. doi:10.1016/j.applthermaleng.2018.10.066.

[10] Gong C, Yi L, Zhang Z, Sun J, Liu F. Assessment of ultra-lean burn characteristics for a stratified-charge direct-injection spark-ignition methanol engine under different high compression ratios. Appl Energy 2020;261:114478. doi:10.1016/j.apenergy.2019.114478.

[11] Zhen X, Li X, Wang Y, Liu D, Tian Z, Wang Y. Effects of the initial flame kernel radius and EGR rate on the performance, combustion and emission of high-compression spark-ignition methanol engine. Fuel 2020;262:116633. doi:10.1016/j.fuel.2019.116633.

[12] Chen B, Xu HR, Sun Q, Zhang HC, Tan P, Cai WZ, He W, Ni M. Syngas/power cogeneration from proton conducting solid oxide fuel cells assisted by dry methane reforming: A thermal-electrochemical modelling study. Energy Conversion and Management 2018; 167: 37-44. doi.org/10.1016/j.enconman.2018.04.078.

[13] Wu Z, Zhang Z, Ni M. Modeling of a novel SOFC-PEMFC hybrid system coupled with thermal swing adsorption for H2 purification: Parametric and exergy analyses. Energy Convers Manag 2018;174:802–13. doi:10.1016/j.enconman.2018.08.073.

[14] Ni M, Shao ZP. Fuel cells that operate at 300^{o} to 500^{o}C. Science 2020; 369(6500): 138-139. DOI: 10.1126/science.abc9136.

[15] Zhang H, Kong W, Dong F, Xu H, Chen B, Ni M. Application of cascading thermoelectric generator and cooler for waste heat recovery from solid oxide fuel cells. Energy Convers Manag 2017;148:1382–90. doi:10.1016/j.enconman.2017.06.089.

[16] Mekhilef S, Saidur R, Safari A. Comparative study of different fuel cell technologies. Renew Sustain Energy Rev 2012;16:981–9. doi:10.1016/j.rser.2011.09.020.

[17] Wu Z, Tan P, Chen B, Cai W, Chen M, Xu X, et al. Dynamic modeling and operation strategy of an NG-fueled SOFC-WGS-TSA-PEMFC hybrid energy conversion system for fuel cell vehicle by using MATLAB/SIMULINK. Energy 2019;175:567–79. doi:10.1016/j.energy.2019.03.119.

[18] Herdem MS, Farhad S, Hamdullahpur F. Modeling and parametric study of a methanol reformate gas-fueled HT-PEMFC system for portable power generation applications. Energy Convers Manag 2015;101:19–29. doi:10.1016/j.enconman.2015.05.004.

[19] Baak JA, Pozarlik AK, Arentsen MJ, Brem G. Techno-economic study of a zero-emission methanol based energy storage system. Energy Convers Manag 2019;182:530–45. doi:10.1016/j.enconman.2018.12.015.

[20] Jiang J, Li Y, Liang J, Yang W, Li X. Modeling of high-efficient direct methanol fuel cells with order-structured catalyst layer. Appl Energy 2019;252:113431. doi:10.1016/j.apenergy.2019.113431.

[21] Hu X-Q, Yang Q-W, Xiao G, Chen X-T, Qiu X. Power generation enhancement in direct methanol fuel cells using non-uniform cross-sectional serpentine channels. Energy Convers Manag 2019;188:438–46. doi:10.1016/j.enconman.2019.03.058.

[22] Xu H, Chen B, Tan P, Cai W, He W, Farrusseng D, et al. Modeling of all porous solid oxide fuel cells. Appl Energy 2018;219:105–13. doi:10.1016/j.apenergy.2018.03.037.

[23] Liao T, He Q, Xu Q, Dai Y, Cheng C, Ni M. Harvesting waste heat produced in solid oxide fuel cell using near-field thermophotovoltaic cell. J Power Sources 2020;452:227831. doi:10.1016/j.jpowsour.2020.227831.

[24] Laosiripojana N, Assabumrungrat S. Catalytic steam reforming of methane, methanol, and ethanol over Ni/YSZ: The possible use of these fuels in internal reforming SOFC. J Power Sources 2007;163:943–51. doi:10.1016/j.jpowsour.2006.10.006.

[25] Liu M, Peng R, Dong D, Gao J, Liu X, Meng G. Direct liquid methanol-fueled solid oxide fuel cell. J Power Sources 2008;185:188–92. doi:10.1016/j.jpowsour.2008.06.076.

[26] Strazza C, Del Borghi A, Costamagna P, Traverso A, Santin M. Comparative LCA of methanol-fuelled SOFCs as auxiliary power systems on-board ships. Appl Energy 2010;87:1670–8. doi:10.1016/j.apenergy.2009.10.012.

[27] Dokamaingam P, Assabumrungrat S, Soottitantawat A, Laosiripojana N. Effect of operating conditions and gas flow patterns on the system performances of IIR-SOFC fueled by methanol. Int J Hydrogen Energy 2009;34:6415–24. doi:10.1016/j.ijhydene.2009.05.105.

[28] McFarlan A. Techno-economic assessment of pathways for electricity generation in northern remote communities in Canada using methanol and dimethyl ether to replace diesel. Renew Sustain Energy Rev 2018;90:863–76. doi:10.1016/j.rser.2018.03.076.

[29] Chen X, Zhou H, Yu Z, Li W, Tang J, Xu C, et al. Thermodynamic and economic assessment of a PEMFC-based micro-CCHP system integrated with geothermal-assisted methanol reforming. Int J Hydrogen Energy 2020;45:958–71. doi:10.1016/j.ijhydene.2019.10.176.

[30] Cocco D, Tola V. Externally reformed solid oxide fuel cell–micro-gas turbine (SOFC–MGT) hybrid systems fueled by methanol and di-methyl-ether (DME). Energy 2009;34:2124–30. doi:10.1016/j.energy.2008.09.013.

[31] Zakaria Z, Kamarudin SK. Direct conversion technologies of methane to methanol: An overview. Renew Sustain Energy Rev 2016;65:250–61. doi:10.1016/j.rser.2016.05.082.

[32] Stiller C, Thorud B, Seljebø S, Mathisen Ø, Karoliussen H, Bolland O. Finite-volume modeling and hybrid-cycle performance of planar and tubular solid oxide fuel cells. J Power Sources 2005;141:227–40. doi:10.1016/j.jpowsour.2004.09.019.

[33] Aguiar P, Adjiman CS, Brandon NP. Anode-supported intermediate temperature direct internal reforming solid oxide fuel cell. I: model-based steady-state performance. J Power Sources 2004;138:120–36. doi:10.1016/j.jpowsour.2004.06.040.

[34] Levenspiel O. Chemical Reaction Engineering. John Wiley and Sons, New York; 1972.

[35] Correa JM, Farret FA, Canha LN, Simoes MG. An Electrochemical-Based Fuel-Cell Model Suitable for Electrical Engineering Automation Approach. IEEE Trans Ind Electron 2004;51:1103–12. doi:10.1109/TIE.2004.834972.

[36] Owebor K, Oko COC, Diemuodeke EO, Ogorure OJ. Thermo-environmental and economic analysis of an integrated municipal waste-to-energy solid oxide fuel cell, gas-, steam-, organic fluid- and absorption refrigeration cycle thermal power plants. Appl Energy 2019;239:1385–401. doi:10.1016/j.apenergy.2019.02.032.

[37] Samanta S, Ghosh S. Techno-economic assessment of a repowering scheme for a coal fired power plant through upstream integration of SOFC and downstream integration of MCFC. Int J Greenh Gas Control 2017;64:234–45. doi:10.1016/j.ijggc.2017.07.020.

[38] Chougule A, Sonde RR. Modelling and experimental investigation of compact packed bed design of methanol steam reformer. Int J Hydrogen Energy 2019;44:29937–45. doi:10.1016/j.ijhydene.2019.09.166.

[39] Thattarathody R, Sheintuch M. Kinetics and dynamics of methanol steam reforming on CuO/ZnO/alumina catalyst. Appl Catal A Gen 2017;540:47–56. doi:10.1016/j.apcata.2017.04.012.

[40] Xiaoru Z, Xinhai X, Xia X, Lun L, Wenfu X. Review of reaction kinetic investigations oon methanol steam reforming for hydrogen production [In Chineses]. Chem Ind Eng Prog 2020;39:152–65. doi:10.16085/j.issn.1000-6613.2019-0432.

[41] Xing S, Zhao C, Ban S, Liu Y, Wang H. Thermodynamic performance analysis of the influence of multi-factor coupling on the methanol steam reforming reaction. Int J Hydrogen Energy 2020;45:7015–24. doi:10.1016/j.ijhydene.2019.12.192.

[42] R.C. Reid. The Properties of Gases and Liquids. New York Mc Graw-Hill Book Company; 1987.

[43] Eveloy V. Hybridization of solid oxide electrolysis-based power-to-methane with oxyfuel combustion and carbon dioxide utilization for energy storage. Renew Sustain Energy Rev 2019;108:550–71. doi:10.1016/j.rser.2019.02.027.

[44] Hajabdollahi Z, Fu P-F. Multi-objective based configuration optimization of SOFC-GT cogeneration plant. Appl Therm Eng 2017;112:549–59. doi:10.1016/j.applthermaleng.2016.10.103.

[45] MUTHUKUMAR P, PRAKASHMAIYA M, MURTHY S. Experiments on a metal hydride-based hydrogen storage device. Int J Hydrogen Energy 2005;30:1569–81. doi:10.1016/j.ijhydene.2004.12.007.

[46] Kyoung S, Ferekh S, Gwak G, Jo A, Ju H. Three-dimensional modeling and simulation of hydrogen desorption in metal hydride hydrogen storage vessels. Int J Hydrogen Energy 2015;40:14322–30. doi:10.1016/j.ijhydene.2015.03.114.

[47] Jemni A. Experimental and theoretical study of ametal–hydrogen reactor. Int J Hydrogen Energy 1999;24:631–44. doi:10.1016/S0360-3199(98)00117-7.

[48] Robledo CB, van Leeuwen LB, van Wijk AJM. Hydrogen fuel cell scooter with plug-out features for combined transport and residential power generation. Int J Hydrogen Energy 2019;44:29648–57. doi:10.1016/j.ijhydene.2019.04.103.

[49] Ferguson JR, Fiard JM, Herbin R. Three-dimensional numerical simulation for various geometries of solid oxide fuel cells. J Power Sources 1996;58:109–22. doi:10.1016/0378-7753(95)02269-4.

[50] Cheddie DF. Integration of A Solid Oxide Fuel Cell into A 10 MW Gas Turbine Power Plant. Energies 2010;3:754–69. doi:10.3390/en3040754.

[51] Ni M, Leung MKH, Leung DYC. Parametric study of solid oxide fuel cell performance. Energy Convers Manag 2007;48:1525–35. doi:10.1016/j.enconman.2006.11.016.

[52] Wu Z, Zhu P, Yao J, Tan P, Xu H, Chen B, et al. Thermo-economic modeling and analysis of an NG-fueled SOFC-WGS-TSA-PEMFC hybrid energy conversion system for stationary electricity power generation. Energy 2020;192:116613. doi:10.1016/j.energy.2019.116613.

[53] Chitsaz A, Mehr AS, Mahmoudi SMS. Exergoeconomic analysis of a trigeneration system driven by a solid oxide fuel cell. Energy Convers Manag 2015;106:921–31. doi:10.1016/j.enconman.2015.10.009.

[54] Sohani A, Naderi S, Torabi F. Comprehensive comparative evaluation of different possible optimization scenarios for a polymer electrolyte membrane fuel cell. Energy Convers Manag 2019;191:247–60. doi:10.1016/j.enconman.2019.04.005.

[55] Marechal F, Palazzi F, Godat J, Favrat D. Thermo-Economic Modelling and Optimisation of Fuel Cell Systems. Fuel Cells 2005;5:5–24. doi:10.1002/fuce.200400055.

[56] Sanusi YS, Mokheimer EMA. Thermo-economic optimization of hydrogen production in a membrane-SMR integrated to ITM-oxy-combustion plant using genetic algorithm. Appl Energy 2019;235:164–76. doi:10.1016/j.apenergy.2018.10.082.

[57] Turton R. Analysis, Synthesis and Design of Chemical Processes. Prentice Hall, NJ; 1998.

[58] Kumar P, Singh O. Thermoeconomic analysis of SOFC-GT-VARS-ORC combined power and cooling system. Int J Hydrogen Energy 2019;44:27575–86. doi:10.1016/j.ijhydene.2019.08.198.

[59] Sartori da Silva F, Matelli JA. Exergoeconomic analysis and determination of power cost in MCFC – steam turbine combined cycle. Int J Hydrogen Energy 2019;44:18293–307. doi:10.1016/j.ijhydene.2019.05.156.

[60] Prakash D, Singh O. Thermo-economic study of combined cycle power plant with carbon capture and methanation. J Clean Prod 2019;231:529–42. doi:10.1016/j.jclepro.2019.05.217.

[61] Feng P, Liu Y, Ayub I, Wu Z, Yang F, Zhang Z. Techno-economic analysis of screening metal hydride pairs for a 910 MWhth thermal energy storage system. Appl Energy 2019;242:148–56. doi:10.1016/j.apenergy.2019.03.046.

[62] Bi Z, Cheng M, Wu H, Dong Y, Yi B. Performance of intermediary temperature solid oxide fuel cell with methanol as fuel [In Chinese]. Chem J Chinese U 2005;26:1110–3.

[63] Kim J. Modeling of Proton Exchange Membrane Fuel Cell Performance with an Empirical Equation. J Electrochem Soc 1995;142:2670. doi:10.1149/1.2050072.

[64] Yang FS, Chen XY, Wu Z, Wang SM, Wang GX, Zhang ZX, et al. Experimental studies on the poisoning properties of a low-plateau hydrogen storage alloy LaNi4.3Al0.7 against CO impurities. Int J Hydrogen Energy 2017;42:16225–34. doi:10.1016/j.ijhydene.2017.05.131.

[65] AH 7500-AH Power Module [In Chinese]. Guangdong Hejide Energy Technol Co,Ltd 2019. http://www.chinahydrogen.cn/page15?_l=en.

[66] Wee J-H. Carbon dioxide emission reduction using molten carbonate fuel cell systems. Renew Sustain Energy Rev 2014;32:178–91. doi:10.1016/j.rser.2014.01.034.

[67] Yang Q-W, Hu X-Q, Zhu Y, Lei X-C, Yu B, Ji S-C. Extended criterion for robustness evaluations of energy conversion efficiency in DMFCs. Energy Convers Manag 2018;172:285–95. doi:10.1016/j.enconman.2018.07.004.

[68] Bai Z, Liu Q, Lei J, Jin H. Investigation on the mid-temperature solar thermochemical power generation system with methanol decomposition. Appl Energy 2018;217:56–65. doi:10.1016/j.apenergy.2018.02.101.

[69] Cheddie DF. Thermo-economic optimization of an indirectly coupled solid oxide fuel cell/gas turbine hybrid power plant. Int J Hydrogen Energy 2011;36:1702–9. doi:10.1016/j.ijhydene.2010.10.089.

[70] Guidelines for the deepening the reform of formation mechanism of feed-in tariff of coal fired power plant [In Chineses]. China Natl Dev Reform Comm 2019. http://www.gov.cn/xinwen/2019-10/25/content_5444655.htm.